Analysis of COVID-19 and comorbidity co-infection model with optimal control

7 authors, including:

Andrew Omame
York University
107 PUBLICATIONS **2,265** CITATIONS

Ndolane Sene
Cheikh Anta Diop University
97 PUBLICATIONS **2,637** CITATIONS

Ikenna Nometa
University of Hawaiʻi at Mānoa
9 PUBLICATIONS **137** CITATIONS

Cosmas Ifeanyi Nwakanma
West Virginia University
238 PUBLICATIONS **2,218** CITATIONS

RESEARCH ARTICLE

WILEY

Analysis of COVID-19 and comorbidity co-infection model with optimal control

Andrew Omame[1] | **Ndolane Sene[2]** | **Ikenna Nometa[3]** |
Cosmas I. Nwakanma[4] | **Emmanuel U. Nwafor[1]** | **Nneka O. Iheonu[1]** |
Daniel Okuonghae[5]

[1]Department of Mathematics, Federal University of Technology Owerri, Owerri, Nigeria

[2]Laboratoire Lmdan, Département de Mathématiques de la Décision, Facultédes Sciences Economiques et Gestion, Université Cheikh Anta Diop de Dakar, Dakar Fann, Senegal

[3]Department of Mathematics, University of Hawaii Manoa, Honolulu, Hawaii, USA

[4]Networked Systems Lab, IT Covergence Engineering, School of Electronic Engineering, Kumoh National Institute of Technology, Gumi, Korea

[5]Department of Mathematics, University of Benin, Benin City, Nigeria

Correspondence
Andrew Omame, Department of Mathematics, Federal University of Technology Owerri, Owerri, Nigeria.
Email: andrew.omame@futo.edu.ng

Abstract

In this work, we develop and analyze a mathematical model for the dynamics of COVID-19 with re-infection in order to assess the impact of prior comorbidity (specifically, **diabetes mellitus**) on COVID-19 complications. The model is simulated using data relevant to the dynamics of the diseases in Lagos, Nigeria, making predictions for the attainment of peak periods in the presence or absence of comorbidity. The model is shown to undergo the phenomenon of backward bifurcation caused by the parameter accounting for increased susceptibility to COVID-19 infection by comorbid susceptibles as well as the rate of reinfection by those who have recovered from a previous COVID-19 infection. Simulations of the cumulative number of active cases (including those with comorbidity), at different reinfection rates, show infection peaks reducing with decreasing reinfection of those who have recovered from a previous COVID-19 infection. In addition, optimal control and cost-effectiveness analysis of the model reveal that the strategy that prevents COVID-19 infection by comorbid susceptibles is the most cost-effective of all the control strategies for the prevention of COVID-19.

KEYWORDS

comorbidity, COVID-19, data-fitting, optimal control, reinfection

1 | INTRODUCTION

The new coronavirus disease 2019 (COVID-19) was reported for the first time in the Chinese city of Wuhan, in the closing month of the year 2019.[1] The disease spread rapidly across the globe like wildfire, that on March 11, 2020, the World Health Organization (WHO) declared it a global pandemic.[2] As of February 19, 2021, the global cases of COVID-19 infection stands at 110,430,962 with 2,444,074 deaths.[3] The morbidity and mortality vary across countries of the world with the highest reported in the United States (27,897,356 confirmed cases with 493,138 deaths), India (10,963,394 confirmed cases with 156,111 deaths), and Brazil (10,030,626 confirmed cases with 243,457 deaths) as of February 19, 2021.[3] COVID-19 "can often present as a common cold-like illness," with other symptoms including fever, fatigue, muscle pains, loss or change of taste or smell, shortness of breath, dry cough, and sore throat.[4] The disease can be spread from person-to-person through the breathing in of respiratory droplets from infected persons and via direct contact with contaminated objects and surfaces.[5]

Recently, vaccines have been approved to mitigate the spread of COVID-19. However, the use of the vaccine is still at the early stage of dissemination and adoption.[6] About 12 COVID-19 vaccines have been approved with efficacies up to 95%, while about 243 others are in various phases of trials.[7,8] Currently, no data is available about the duration of protection from the available vaccines, although studies are currently underway in this respect.[9] Presently, there is no stated approved antiviral treatment for COVID-19. Governments of different nations and individuals have embarked on non-pharmaceutical interventions such as face mask usage in the public and social distancing observance as a means of effectively reducing the spread of the disease.[10,11]

Individuals with previous comorbidity (such as diabetes, lung disease, and heart disease) are more likely to develop severe illness with stronger COVID-19 symptoms than those without comorbidity.[2] Bjorgul et al.[12] defined comorbidities as "diseases or medical conditions unrelated in etiology or causality to the principal diagnosis that coexist with the disease of interest." According to the Centres for Disease Control and prevention (CDC) "People of any age with the following conditions are at increased risk of severe illness from COVID-19: Chronic kidney disease, COPD (chronic obstructive pulmonary disease), Immunocompromised state (weakened immune system) from solid organ transplant, Obesity (body mass index [BMI] of 30 or higher), Serious heart conditions, such as heart failure, coronary artery disease, or cardiomyopathies, Sickle cell disease, Type 2 diabetes mellitus (DM), Hypertension or high blood pressure and Neurologic conditions, such as dementia."[13] This is further confirmed by a clinical report by Huang et al.[14] who in a survey of 41 confirmed COVID-19 patients discovered that 13 of them had underlying diseases, which include, hypertension, chronic obstructive pulmonary disease cardiovascular disease, and diabetes. Furthermore, Wang et al. reported from a finding involving 138 patients, that over 45% of them had one or more comorbidities and that "the patients who were admitted to the intensive care unit (ICU) had a higher number of comorbidities (72.2%) than those not admitted to the ICU (37.3%)."[15,16]

In Nigeria, the Ministry of Health had reported that prior comorbid conditions such as DM, tuberculosis, and hypertension were responsible for about 70% of COVID-19-related deaths.[17] Recent studies carried out in Nigeria estimated the prevalence of DM to range from lowest level of 0.8% among adults in rural settings to over 7% in urban Lagos with an average of 2.2% nationally.[18] DM has been reported to increase the vulnerability of individuals to infection with COVID-19.[19] The prevalence of DM is higher in patients with severe COVID-19 disease than in patients with mild symptoms.[19] Badawi and Ryoo[20] reported that patients with DM have increased susceptibility to viral and bacterial infections including those affecting the respiratory tract. In another study, Carey et al.[21] found out that both type 1 and type 2 diabetes increase the susceptibility to infections and their complications. More recently, WHO has warned that currently no evidence to show that those who have recovered from COVID-19 infection can not get reinfected.[22] On April 13, 2020, South Korea reported that more than 100 of its recovered cases of COVID-19 have been reinfected again.[23] This calls for serious concern as several countries, including China and South Korea, which had previously recorded giant strides in curbing the virus, have recently reported second waves of COVID-19 infections.[24,25]

Mathematical modeling has been a powerful means of studying the behaviour of infectious diseases.[26-40] A lot of models have been developed for the dynamics of COVID-19.[41-45] For instance, the authors in Reference 44 developed and analyzed a mathematical model for COVID-19 population dynamics in Lagos, Nigeria. Simulations of the model showed that if at least 55% of the population comply with the social distancing regulation with about 55% of the population effectively making use of face masks while in public, the disease will eventually die out in the population and that, if the case detection rate for symptomatic individuals can be increased to about 0.8 per day, with about 55% of the population complying with the social distancing regulations, it will result to a great reduction in the incidence of the disease. Asamoah et al.[45] investigated the global stability analysis of COVID-19 assessing the impact of environment, using data from Ghana. Results from the analyses of the model showed that reinfection is possible after recovery and that the strategy that cleans environmental surfaces with home-based detergents is the most cost-effective strategy in the control of COVID-19 infection. Also, in a related paper, Nkwayep et al.[46] investigated short-term forecasts of COVID-19 pandemics in Cameroon. They showed that facemask usage alone is not sufficient to contain the spread of the virus. However, the pandemic could quickly disappear from the population if more effective control strategies such as containment, face-mask usage by individuals in public and the social distancing rules are combined and effectively enforced.

In this study, we shall be investigating the impact of reinfection and co-infection with comorbidity on the dynamics of COVID-19 disease. In addition, we shall be carrying out optimal control analysis on the model to assess the impact of some control strategies on the prevention of COVID-19. Specifically, the comorbidity of interest for this study shall be DM.

The paper is organized as follows. The model formulation and basic properties of the model are reported in Section 2. The model (without controls) is analyzed (qualitatively and quantitatively) in Sections 3and 4. Optimal control analysis is carried out in Section 5 while Section 6 gives the concluding remarks.

2 | MODEL FORMULATION

The total population at time t, denoted by $N_h(t)$, is divided into eight mutually exclusive compartments: Susceptible individuals ($S_h(t)$), comorbid susceptible individuals (S_{cm}), non-comorbid individuals with COVID-19 infection ($I_{cv}(t)$), non-comorbid isolated and hospitalized individuals infected with COVID-19 ($Q_{cv}(t)$), individuals who have recovered from COVID-19 infection ($R_{cv}(t)$), individuals co-infected with COVID-19 and comorbidity ($I_{cvcm}(t)$), isolated and hospitalized individuals co-infected with COVID-19 infection and comorbidity (Q_{cvcm}), individuals who have recovered from COVID-19 infection but with comorbidity (R_{cm}). Susceptible individuals acquire COVID-19 infection at the rate

$$\lambda_{CV} = \frac{\beta_{CV}(I_{CV} + I_{CVCM})}{N_H}.$$

It is assumed that, susceptible individuals acquire comorbidity at the rate θ_{CM}. Comorbid susceptible individuals acquire COVID-19 infection at an increased rate $\chi_{CM}\lambda_{CV}$, with $\chi_{CM} > 1$.[20,21] Natural death occurs in all compartments at the rate μ_H.

The total population at time, t is given by

$$N_H = S_H + S_{CM} + I_{CV} + Q_{CV} + R_{CV} + I_{CVCM} + Q_{CVCM} + R_{CVCM}.$$

Based on the above formulations and assumptions, the COVID-19 and comorbidity co-infection model is given by the system of nonlinear deterministic differential equations (flow diagram of the model is shown in Figure 1, the associated state variables and parameters are well described in Table 1) given below:

$$\frac{dS_H}{dt} = \Lambda_H - (\lambda_{CV} + \theta_{CM} + \mu_H)S_H,$$

$$\frac{dS_{CM}}{dt} = \theta_{CM}S_H - \chi_{CM}\lambda_{CV}S_{CM} - \mu_H S_{CM},$$

$$\frac{dI_{CV}}{dt} = \lambda_{CV}S_H - (\eta_1 + \varphi_{I1} + \mu_H)I_{CV} + \psi_1\lambda_{CV}R_{CV},$$

$$\frac{dQ_{CV}}{dt} = \eta_1 I_{CV} - (\varphi_{Q1} + \delta_1 + \mu_H)Q_{CV},$$

$$\frac{dR_{CV}}{dt} = \varphi_{I1}I_{CV} + \varphi_{Q1}Q_{CV} - \mu_H R_{CV} - \psi_1\lambda_{CV}R_{CV},$$
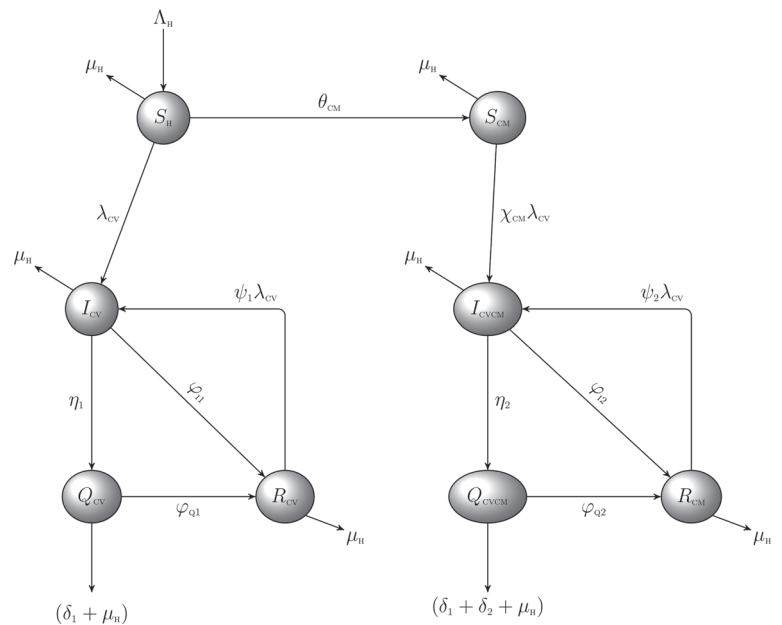

FIGURE 1 Schematic diagram of the model (1) where $\lambda_{CV} = \frac{\beta_{CV}(I_{CV}+I_{CVCM})}{N_H}$

TABLE 1 Description of variables and parameters in the model equation

Variable	Interpretation
S_h	Susceptible humans
S_{cm}	Comorbid susceptible individuals
I_{cv}	Individuals singly infected with COVID-19
Q_{cv}	infectious individuals isolated and hospitalized for COVID-19 treatment
R_{cv}	Individuals who have recovered from COVID-19 infection
I_{cvcm}	Individuals co-infected with COVID-19 and comorbidity
Q_{cvcm}	Isolated and hospitalized individuals co-infected with COVID-19 and comorbidity
R_{cm}	Individuals who have recovered from COVID-19 but with comorbidity
Parameter	**Interpretation**
Λ_H	Recruitment rate
μ_H	Natural death rate
β_{CV}	Effective contact rate for COVID-19 transmission
θ_{CM}	Rate of comorbidity development by susceptible humans
η_1, η_2	Detection rates for compartments I_{cv} and I_{cvcm}, respectively
$\varphi_{i1}, \varphi_{q1}, \varphi_{i2}, \varphi_{q2}$	Recovery rates from COVID-19 for individuals in compartments I_{cv}, Q_{cv}, I_{cvcm} and Q_{cvcm}, respectively
δ_1	COVID-19-induced death rate for infected individuals in I_{cv} and Q_{cvcm} compartments, respectively
δ_2	Comorbidity-induced death rate for infected individuals in Q_{cvcm} compartment
ψ_1, ψ_2	Reinfection rates for individuals who have recovered from COVID-19 In compartments R_{cv} and R_{cm}
χ_{CM}	Modification parameter accounting for increased susceptibility to COVID-19 Infection by comorbid susceptibles

$$\frac{dI_{CVCM}}{dt} = \chi_{CM}\lambda_{CV}S_{CM} - (\eta_2 + \varphi_{I2} + \mu_H)I_{CVCM} + \psi_2\lambda_{CV}R_{CM},$$

$$\frac{dQ_{CVCM}}{dt} = \eta_2 I_{CVCM} - (\delta_1 + \delta_2 + \varphi_{Q2} + \mu_H)Q_{CVCM},$$

$$\frac{dR_{CM}}{dt} = \varphi_{I2}I_{CVCM} + \varphi_{Q2}Q_{CVCM} - \mu_H R_{CM} - \psi_2\lambda_{CV}R_{CM}, \tag{1}$$

with

$$\lambda_{CV} = \frac{\beta_{CV}(I_{CV} + I_{CVCM})}{N_H}.$$

2.1 | Basic properties of the model

2.1.1 | Positivity and boundedness

For the model (1) to be epidemiologically meaningful, it is important to prove that all its state variables are nonnegative for all time (t).

Theorem 1. *Let the initial data $S_h > 0, S_{cm} > 0, I_{cv} > 0, Q_{cv} > 0, R_{cv} > 0, I_{cvcm} > 0, Q_{cvcm} > 0, R_{cm} > 0$. Then the solutions $(S_h, S_{cm}, I_{cv}, Q_{cv}, R_{cv}, I_{cvcm}, Q_{cvcm}, R_{cm})$ of the model (1) are positive for all time $t > 0$.*

Proof. Let

$t_1 = \sup\{t > 0 : S_H > 0, S_{CM} > 0, I_{CV} > 0, Q_{CV} > 0, R_{CV} > 0, I_{CVCM} > 0, Q_{CVCM} > 0, R_{CM} > 0\}$. Thus, $t_1 > 0$.

We have, from the first equation of the system (1) that

$$\frac{dS_H}{dt} = \Lambda_H - (\lambda_{CV} + \theta_{CM} + \mu_H)S_H,$$

which can be rewritten as

$$\frac{d}{dt}\left\{S_H(t)\exp\left[\int_0^t \lambda_{CV}(u)du + \theta_{CM}t + \mu_H t\right]\right\} = \Lambda_H \exp\left[\int_0^t \lambda_{CV}(u)du + \theta_{CM}t + \mu_H t\right],$$

so that

$$\left\{S_H(t_1)\exp\left[\int_0^{t_1} \lambda_{CV}(u)du + \theta_{CM}t_1 + \mu_H t_1\right]\right\} - S_H(0) = \Lambda_H \int_0^{t_1} \exp\left[\int_0^x \lambda_{CV}(u)du + \theta_{CM}x + \mu_H x\right]dx,$$

so that

$$S_H(t_1) = S_H(0)\exp\left[-\int_0^{t_1} \lambda_{CV}(u)du - \theta_{CM}t_1 - \mu_H t_1\right] + \exp\left[-\int_0^{t_1} \lambda_{CV}(u)du - \theta_{CM}t_1 - \mu_H t_1\right]$$
$$\times \Lambda_H \int_0^{t_1} \exp\left[\int_0^x \lambda_{CV}(u)du + \theta_{CM}x + \mu_H x\right]dx > 0.$$

In a similar manner, it can be proven that:
$S_{cm} > 0, I_{cv} > 0, Q_{cv} > 0, R_{cv} > 0, I_{cvcm} > 0, Q_{cvcm} > 0, R_{cm} > 0.$ ∎

2.2 | Invariant regions

The co-infection model (1) will be analyzed in a biologically feasible region as follows. We first show that the system (1) is dissipative in a proper subset $\mathcal{D} \subset \mathfrak{R}_+^8$. Let

$$\mathcal{D} = \left\{(S_H, S_{CM}, I_{CV}, Q_{CV}, R_{CV}, I_{CVCM}, Q_{CVCM}, R_{CM}) \in \mathfrak{R}_+^8 : S_H + S_{CM} + I_{CV} + Q_{CV} + R_{CV} + I_{CVCM} + Q_{CVCM} + R_{CM} \le \frac{\Lambda_H}{\mu_H}\right\}.$$

The following steps are followed to establish the positive invariance of $\mathcal{D}$.

Adding all the equations of the system (1) gives

$$\frac{dN_H}{dt} = \Lambda_H - \mu_H N_H(t) - [\delta_1(Q_{CV} + Q_{CVCM}) + \delta_2 Q_{CVCM}]. \tag{2}$$

From (2), we have that

$$\Lambda_H - (\mu_H + 3\delta_H)N_H \le \frac{dN_H}{dt} < \Lambda_H - \mu_H N_H,$$

where $\delta_H = \min\{\delta_1, \delta_2\}$.

Using the Comparison theorem,[47] we have that, $N_H(t) \le \frac{\Lambda_H}{\mu_H}$ if $N_H(0) \le \frac{\Lambda_H}{\mu_H}$. Thus, the region $\mathcal{D}$ is positively invariant. Hence, it is sufficient to consider the dynamics of the flow generated by the system (1) in $\mathcal{D}$. Thus, within this region, the model (1) is said to be epidemiologically and mathematically well-posed.[48] Thus, every solution of the model (1) with initial conditions in $\mathcal{D}$ remains in $\mathcal{D}$ for all time $t \ge 0$. Therefore, the $\omega-$limit sets of the system (1) are contained in $\mathcal{D}$. This result is summarized thus.

Lemma 1. *The region $\mathcal{D} \subset \mathfrak{R}_+^8$ is positively invariant for the model (1) with initial conditions in $\mathfrak{R}_+^8$.*

3 | ANALYSIS OF THE MODEL WITHOUT CONTROLS

In this section, we seek to qualitatively study the dynamical properties of the model (1) without controls.

3.1 | Basic reproduction number of the co-infection model (1)

The COVID-19-comorbidity co-infection model (1) has a COVID-19-free equilibrium (CFE), obtained by setting the disease classes and the right-hand sides of the equations in the model (1) to zero, given by

$$
\begin{aligned}
\xi_0 &= (S_H^*, S_{CM}^*, I_{CV}^*, Q_{CV}^*, R_{CV}^*, I_{CVCM}^*, Q_{CVCM}^*, R_{CM}^*) \\
&= \left(\frac{\Lambda_H}{(\mu_H + \theta_{CM})}, \frac{\theta_{CM}\Lambda_H}{\mu_H(\mu_H + \theta_{CM})}, 0, 0, 0, 0, 0, 0 \right).
\end{aligned}
\tag{3}
$$

The basic reproduction number of the co-infection model (1), using the approach illustrated in Reference 49, is given by

$$
\mathcal{R}_{0C} = \beta_{CV} \left(\frac{S_H^*}{N_H^*(\eta_1 + \varphi_{I1} + \mu_H)} + \frac{\chi_{CM} S_{CM}^*}{N_H^*(\eta_2 + \varphi_{I2} + \mu_H)} \right).
$$

3.2 | Local asymptotic stability of the CFE of the co-infection model

Theorem 2. *The CFE, ξ_0, of the model (1) is locally asymptotically stable (LAS) if $\mathcal{R}_{0C} < 1$, and unstable if $\mathcal{R}_{0C} > 1$.*

Proof. The local stability of the model (1) is analyzed by the Jacobian matrix of the system (1) evaluated at the CFE ξ_0, given by:

$$
\begin{pmatrix}
-\mu_H & 0 & -\frac{\beta_{CV}\mu_H}{\mu_H+\theta_{CM}} & 0 & 0 & -\frac{\beta_{CV}\mu_H}{\mu_H+\theta_{CM}} & 0 & 0 \\
\theta_{CM} & -\mu_H & -\frac{\beta_{CV}\chi_{CM}\theta_{CM}}{\mu_H+\theta_{CM}} & 0 & 0 & -\frac{\beta_{CV}\chi_{CM}\theta_{CM}}{\mu_H+\theta_{CM}} & 0 & 0 \\
0 & 0 & \frac{\beta_{CV}\mu_H}{\mu_H+\theta_{CM}} - K_1 & 0 & 0 & \frac{\beta_{CV}\mu_H}{\mu_H+\theta_{CM}} & 0 & 0 \\
0 & 0 & \eta_1 & -K_2 & 0 & 0 & 0 & 0 \\
0 & 0 & \varphi_{I1} & \varphi_{Q1} & -\mu_H & 0 & 0 & 0 \\
0 & 0 & \frac{\beta_{CV}\chi_{CM}\theta_{CM}}{\mu_H+\theta_{CM}} & 0 & 0 & \frac{\beta_{CV}\chi_{CM}\theta_{CM}}{\mu_H+\theta_{CM}} - K_3 & 0 & 0 \\
0 & 0 & 0 & 0 & 0 & \eta_2 & -K_4 & 0 \\
0 & 0 & 0 & 0 & 0 & \varphi_{I2} & \varphi_{Q2} & -\mu_H
\end{pmatrix},
$$

where, $K_1 = \eta_1 + \varphi_{I1} + \mu_H, K_2 = \varphi_{Q1} + \delta_1 + \mu_H, K_3 = \eta_2 + \varphi_{I2} + \mu_H, K_4 = \varphi_{Q2} + \delta_1 + \delta_2 + \mu_H$.

The eigenvalues are given by $\lambda_1 = -(\eta_1 + \varphi_{I1} + \mu_H), \lambda_2 = -(\varphi_{Q1} + \delta_1 + \mu_H), \lambda_3 = -(\eta_2 + \varphi_{I2} + \mu_H), \lambda_4 = -(\varphi_{Q1} + \delta_1 + \delta_2 + \mu_H)$ and the solutions of the characteristic polynomial

$$
\lambda^2 + \left(K_1 + K_3 - \left(\frac{\beta_{CV}\mu_H}{\mu_H + \theta_{CM}} + \frac{\beta_{CV}\chi_{CM}\theta_{CM}}{\mu_H + \theta_{CM}} \right) \right) \lambda + K_1 K_3 (1 - \mathcal{R}_{0C}) = 0.
\tag{4}
$$

Applying the Routh–Hurwitz criterion, the quadratic Equation (4) will have roots with negative real parts if and only if $\mathcal{R}_{0C} < 1$. As a result, the CFE, ξ_0 is LAS if $\mathcal{R}_{0C} < 1$. ∎

The epidemiological implication of Theorem 2 is that COVID-19 can be eliminated from the population when $\mathcal{R}_{0C} < 1$ and if the initial sizes of the population of the model are in the region of attraction of the CFE.

3.3 | Existence of endemic equilibrium points of the model

In this section, we shall investigate the existence of an endemic equilibrium of the model (1).

Let an arbitrary equilibrium point of the model be given by

$$\xi_e = (S_H^{**}, S_{CM}^{**}, I_{CV}^{**}, Q_{CV}^{**}, R_{CV}^{**}, I_{CVCM}^{**}, Q_{CVCM}^{**}, R_{CM}^{**}).$$

Let

$$\lambda_{CV}^{**} = \frac{\beta_{CV}(I_{CV}^{**} + I_{CVCM}^{**})}{N_H^{**}}. \tag{5}$$

be the force of infection at the endemic steady-state.

The steady-state solutions of equations of the model (1)

$$S_H^{**} = \frac{\Lambda_H}{(\lambda_{CV}^{**} + \theta_{CM} + \mu_H)}, \quad S_{CM}^{**} = \frac{\theta_{CM}\Lambda_H}{(\chi_{CM}\lambda_{CV}^{**} + \mu_H)(\lambda_{CV}^{**} + \theta_{CM} + \mu_H)},$$

$$I_{CV}^{**} = \frac{\Lambda_H\lambda_{CV}^{**}(\mu_H + \psi_1\lambda_{CV}^{**})K_2}{(\lambda_{CV}^{**} + \theta_{CM} + \mu_H)[K_1K_2\mu_H + (\mu_H\psi_1K_2 + \eta_1\psi_1(\delta_1 + \mu_H))\lambda_{CV}^{**}]},$$

$$Q_{CV}^{**} = \frac{\Lambda_H\lambda_{CV}^{**}\eta_1(\mu_H + \psi_1\lambda_{CV}^{**})}{(\lambda_{CV}^{**} + \theta_{CM} + \mu_H)[K_1K_2\mu_H + (\mu_H\psi_1K_2 + \eta_1\psi_1(\delta_1 + \mu_H))\lambda_{CV}^{**}]},$$

$$R_{CV}^{**} = \frac{\Lambda_H\lambda_{CV}^{**}(\varphi_{I1}K_2 + \varphi_{Q1}\eta_1)}{(\lambda_{CV}^{**} + \theta_{CM} + \mu_H)[K_1K_2\mu_H + (\mu_H\psi_1K_2 + \eta_1\psi_1(\delta_1 + \mu_H))\lambda_{CV}^{**}]},$$

$$I_{CVCM}^{**} = \frac{\chi_{CM}\theta_{CM}\Lambda_H\lambda_{CV}^{**}(\mu_H + \psi_2\lambda_{CV}^{**})K_4}{(\lambda_{CV}^{**} + \theta_{CM} + \mu_H)(\chi_{CM}\lambda_{CV}^{**} + \mu_H)[K_3K_4\mu_H + (\mu_H\psi_2K_4 + \eta_2\psi_2(\delta_1 + \delta_2 + \mu_H))\lambda_{CV}^{**}]},$$

$$Q_{CVCM}^{**} = \frac{\chi_{CM}\theta_{CM}\Lambda_H\lambda_{CV}^{**}\eta_2(\mu_H + \psi_2\lambda_{CV}^{**})}{(\lambda_{CV}^{**} + \theta_{CM} + \mu_H)(\chi_{CM}\lambda_{CV}^{**} + \mu_H)[K_3K_4\mu_H + (\mu_H\psi_2K_4 + \eta_2\psi_2(\delta_1 + \delta_2 + \mu_H))\lambda_{CV}^{**}]},$$

$$R_{CVCM}^{**} = \frac{\chi_{CM}\theta_{CM}\Lambda_H\lambda_{CV}^{**}(\varphi_{I2}K_4 + \varphi_{Q2}\eta_2)}{(\lambda_{CV}^{**} + \theta_{CM} + \mu_H)(\chi_{CM}\lambda_{CV}^{**} + \mu_H)[K_3K_4\mu_H + (\mu_H\psi_2K_4 + \eta_2\psi_2(\delta_1 + \delta_2 + \mu_H))\lambda_{CV}^{**}]}. \tag{6}$$

Substituting the above expressions into the force of infection (5), at steady state, gives the following polynomial

$$Q_1(\lambda_{CV}^{**})^4 + Q_2(\lambda_{CV}^{**})^3 + Q_3(\lambda_{CV}^{**})^2 + Q_4\lambda_{CV}^{**} + Q_5 = 0, \tag{7}$$

where

$Q_1 = (\mu_H K_4\psi_2 + \eta_2\psi_2(\delta_1 + \delta_2 + \mu_H))(\psi_1\chi_{CM}K_2 + \psi_1\chi_D\eta_1) > 0,$

$Q_2 = K_2K_4\mu_H^2\psi_1\psi_2 + K_2\mu_H\eta_2(\delta_1 + \delta_2 + \mu_H)\psi_1\psi_2 + K_4\mu_H\eta_1(\delta_1 + \mu_H)\psi_1\psi_2 + \eta_1\eta_2(\delta_1 + \mu_H)(\delta_1 + \delta_2 + \mu_H)\psi_1\psi_2$

$\quad + K_3K_4\mu_H(\psi_1\chi_{CM}K_2 + \psi_1\chi_{CM}\eta_1) + (\mu_H\psi_2K_4 + \eta_2\psi_2(\delta_1 + \delta_2 + \mu_H))(\mu_H\psi_1K_2 + \mu_H\chi_{CM}K_2 + \mu_H\psi_1\eta_1 + \mu_H\chi_{CM}\eta_1$

$\quad + \varphi_{I1}\chi_{CM}K_2 + \varphi_{Q1}\eta_1\chi_{CM}) + (\mu_H\psi_1K_2 + \eta_1\psi_1(\delta_1 + \mu_H))(\psi_2K_4 + \eta_2\psi_2)\theta_{CM}\chi_{CM} - \beta_{CV}\psi_1\chi_{CM}K_2(\mu_H\psi_2K_4$

$\quad + \eta_2\psi_2(\delta_1 + \delta_2 + \mu_H)),$

$Q_3 = (\mu_H + \theta_{CM})K_2K_4\mu_H^2\psi_1\psi_2 + (\mu_H + \theta_{CM})\mu_H\eta_2K_2(\delta_1 + \delta_2 + \mu_H)\psi_1\psi_2 + (\mu_H + \theta_{CM})\mu_H\eta_1K_4(\delta_1 + \mu_H)\psi_1\psi_2$

$\quad + (\mu_H + \theta_{CM})\eta_1\eta_2(\delta_1 + \mu_H)(\delta_1 + \delta_2 + \mu_H)\psi_1\psi_2 + \chi_{CM}\mu_H^2\psi_2K_1K_2K_4 + \chi_{CM}\mu_H\eta_2\psi_2(\delta_1 + \delta_2 + \mu_H) + \chi_{CM}\mu_H^2\psi_1K_2K_3K_4$

$\quad + \chi_{CM}\mu_H\eta_1\psi_1K_3K_4(\delta_1 + \mu_H) + \mu_H^2(\psi_1 + \chi_{CM})K_2K_3K_4 + K_3K_4\mu_H^2\eta_1(\psi_1 + \chi_{CM}) + K_3K_4\chi_{CM}(K_2\varphi_{I1} + \mu_H\varphi_{Q1}\eta_1)$

$\quad + (\mu_H\psi_2K_4 + \eta_2\psi_2(\delta_1 + \delta_2 + \mu_H))(\mu_H^2K_2K\mu_H^2\eta_1 + \mu_H\varphi_{I1}K_2 + \varphi_{Q1}\eta_1\mu_H) + \mu_H\psi_2K_1K_2\theta_{CM}\chi_{CM}(K_4 + \eta_2)$

$\quad + (\mu_H\psi_1K_2 + \eta_1\psi_1\delta_1 + \eta_1\psi_1\mu_H)(\theta_{CM}\chi_{CM}\mu_H K_4 + \theta_{CM}\chi_{CM}\eta_2\mu_H + \theta_{CM}\chi_{CM}\varphi_{I2}K_4\theta_{CM}\chi_{CM}\varphi_{Q2}\eta_2)$

$\quad - \beta_{CV}\psi_1\chi_{CM}\mu_H K_2K_3K_4$

$\quad - \beta_{CV}\mu_H K_2(\chi_{CM} + \psi_1)(\mu_H\psi_2K_4 + \eta_2\psi_2(\delta_1 + \delta_2 + \mu_H)) - \beta_{CV}\theta_{CM}\psi_2K_4(\mu_H\psi_1K_2 + \eta_1\psi_1\chi_{CM}(\delta_1 + \mu_H)),$

$$Q_4 = (\mu_H + \theta_{CM})\mu_H^2\psi_2 K_1 K_2 K_4 + \mu_H \eta_2 \psi_2 K_1 K_2 (\mu_H + \theta_{CM})(\delta_1 + \delta_2 + \mu_H) + \mu_H^2 \psi_1 K_2 K_3 K_4 (\mu_H + \theta_{CM})$$

$$+ (\mu_H + \theta_{CM})\mu_H \eta_1 \psi_1 (\delta_1 + \mu_H) + \chi_{CM}\mu_H^2 K_1 K_2 K_3 K_4 + \mu_H K_3 K_4 \left(\mu_H^2 K_2 + \mu_H^2 \eta_1 + \varphi_{I1}\mu_H K_2 + \varphi_{Q2}\eta_1\mu_H\right)$$

$$+ \mu_H^2 \chi_{CM}\theta_{CM} K_1 K_2 K_4 + \chi_{CM}\theta_{CM}\eta_2 K_1 K_2$$

$$+ \mu_H \chi_{CM}\theta_{CM}\varphi_{Q2}\eta_2 K_1 K_2 - \beta_{CV}\mu_H^3\psi_1 K_2 K_4 - \beta_{CV}\mu_H^2\psi_2\eta_2 K_2 (\delta_1 + \delta_2 + \mu_H) - \beta_{CV}\mu_H^2 K_2 K_3 K_4 \chi_{CM}$$

$$- \beta_{CV}\mu_H^2\psi_1 K_2 K_3 K_4 - \beta_{CV}\chi_{CM}\theta_{CM}\mu_H K_4 (\mu_H \psi_1 K_2 + \eta_1 \psi_1 \delta_1 + \eta_1 \psi_1 \mu_H)$$

$$- \beta_{CV}\chi_{CM}\theta_{CM}\psi_2\mu_H K_1 K_2 K_4,$$

$$Q_5 = (\mu_H + \theta_{CM})K_1 K_2 K_3 K_4 \mu_H^2 (1 - \mathcal{R}_{0C}). \tag{8}$$

The components of the endemic equilibrium point (EEP) are obtained upon solving for λ_{CV}^{**} from the polynomial (7), and substituting the positive values of λ_{CV}^{**} into the expressions in (6). Moreover, it follows from (8) that the coefficient Q_1 is always positive, and Q_5 is positive (negative) if $\mathcal{R}_{0C}$ is less (greater) than one. The following results can be deduced.

Theorem 3. *The model (1) has:*

(i) *four or two endemic equilibria if $Q_2 > 0, Q_3 < 0, Q_4 > 0$ and $\mathcal{R}_{0C} < 1$,*
(ii) *two endemic equilibria if $Q_2 > 0, Q_3 > 0, Q_4 < 0$ and $\mathcal{R}_{0C} < 1$,*
(iii) *no endemic equilibrium otherwise, if $\mathcal{R}_{0C} < 1$.*

The first two items of Theorem 3 ((i) - (ii)) suggest the possibility of backward bifurcation in the model (1) when $\mathcal{R}_{0C} <$ 1. It is worthy of note to show that, setting the parameters $\psi_1 = \psi_2 = \chi_{CM} = 0$, reduces the quartic (7) to $\mu_H K_3 K_4 (\mu_H^2 K_2 + \mu_H^2\eta_1 + \varphi_{I1}\mu_H K_2 + \varphi_{Q2}\eta_1\mu_H)\lambda_{CV}^{**} + (\mu_H + \theta_{CM})K_1 K_2 K_3 K_4 \mu_H^2 (1 - \mathcal{R}_{0C}) = 0$, resulting in no sign changes in the polynomial equation for $\mathcal{R}_{0C} < 1$. However, for $\mathcal{R}_{0C} < 1$ a unique endemic equilibrium exists. In the subsequent section, we shall explore the existence of the phenomenon of backward bifurcation in the model (1).

3.4 | Backward bifurcation analysis of the model (1)

In this section, we shall seek to determine the type of bifurcation the model (1) will exhibit, using the Center Manifold theory presented by Castillo-Chavez and Song.[50] We establish the result below

Theorem 4. *The model (1) exhibits backward bifurcation at $\mathcal{R}_{0C} = 1$ whenever a bifurcation coefficient, a, defined below, is positive.*

$$a = -\frac{2\beta_{CV}^*(x_1^* v_3 + x_2^* v_6)}{N_H^{*2}}(\omega_3 + \omega_6)(\omega_1 + \omega_2 + \omega_3 + \omega_4\omega_5 + \omega_6 + \omega_7 + \omega_8)$$

$$+ \frac{2\beta_{CV}^*(\omega_3 + \omega_6)}{N_H^*}((\omega_1 + \psi_1\omega_5)v_3 + (\omega_2 + \psi_2\omega_8)v_6).$$

Proof. Suppose

$$\xi_e = (S_H^{**}, S_{CM}^{**}, I_{CV}^{**}, Q_{CV}^{**}, R_{CV}^{**}, I_{CVCM}^{**}, Q_{CVCM}^{**}, R_{CM}^{**}),$$

represents any arbitrary endemic equilibrium of the model. To apply the Center Manifold theory, it is important we carry out the change of variables below.

Let

$$S_H = x_1, S_{CM} = x_2, I_{CV} = x_3, Q_{CV} = x_4, R_{CV} = x_5, I_{CVCM} = x_6, Q_{CVCM} = x_7, R_{CM} = x_8.$$

Moreover, using the vector notation

$$X = (x_1, x_2, x_3, x_4, x_5, x_6, x_7, x_8)^T,$$

the model (1) can be rewritten in the form

$$\frac{dX}{dt} = f = (f_1, f_2, f_3, f_4, f_5, f_6, f_7, f_8)^T,$$

as follows:

$$\frac{dx_1}{dt} = \Lambda_H - (\lambda_{CV} + \theta_{CM} + \mu_H)x_1,$$

$$\frac{dx_2}{dt} = \theta_{CM}x_1 - \chi_{CM}\lambda_{CV}x_2 - \mu_H x_2,$$

$$\frac{dx_3}{dt} = \lambda_{CV}x_1 - (\eta_1 + \varphi_{I1} + \mu_H)x_3 + \psi_1\lambda_{CV}x_5,$$

$$\frac{dx_4}{dt} = \eta_1 x_3 - (\varphi_{Q1} + \delta_1 + \mu_H)x_4,$$

$$\frac{dx_5}{dt} = \varphi_{I1}x_3 + \varphi_{Q1}x_4 - \mu_H x_5 - \psi_1\lambda_{CV}x_5,$$

$$\frac{dx_6}{dt} = \chi_{CM}\lambda_{CV}x_2 - (\eta_2 + \varphi_{I2} + \mu_H)x_6 + \psi_2\lambda_{CV}x_8,$$

$$\frac{dx_7}{dt} = \eta_2 x_6 - (\delta_1 + \delta_2 + \varphi_{Q2} + \mu_H)x_7,$$

$$\frac{dx_8}{dt} = \varphi_{I2}x_6 + \varphi_{Q2}x_7 - \mu_H x_8 - \psi_2\lambda_{CV}x_8, \tag{9}$$

with

$$\lambda_{CV} = \frac{\beta_{CV}(x_3 + x_6)}{\sum_{i=1}^{8} x_i}.$$

Consider the case when $\mathcal{R}_{0C} = 1$. Moreover, let β_{CV} be chosen as a bifurcation parameter. Solving for $\beta_{CV} = \beta_{CV}^*$ from $\mathcal{R}_{0C} = 1$ we obtain

$$\beta_{CV} = \beta_{CV}^* = \frac{K_1 K_3(\mu_H + \theta_{CM})}{(\mu_H K_3 + \chi_{CM}\theta_{CM}K_1)}.$$

Evaluating the Jacobian of the system (1) at the CFE, $J(\xi_0)$, and evaluating the right eigenvector, $\mathbf{w} = [\omega_1, \omega_2, \omega_3, \omega_4, \omega_5, \omega_6, \omega_7, \omega_8]^T$, associated with the simple zero eigenvalue of $J(\xi_0)$, gives

$$\omega_1 = -\frac{K_1 K_3 \Lambda_H(\omega_3 + \omega_6)}{(\mu_H K_3 + \chi_{CM}\theta_{CM}K_1)} < 0, \quad \omega_2 = \frac{K_1 K_3 \theta_{CM}(\Lambda_H + \chi_{CM})(\omega_3 + \omega_6)}{(\mu_H K_3 + \chi_{CM}\theta_{CM}K_1)} > 0, \quad \omega_3 = \omega_3 > 0,$$

$$\omega_4 = \frac{\eta_1 \omega_3}{K_2} > 0, \quad \omega_5 = \frac{(\varphi_{I1}K_2 + \varphi_{Q1}\eta_1)\omega_3}{\mu_H K_2} > 0, \quad \omega_6 = \omega_6 > 0, \quad \omega_7 = \frac{\eta_2 \omega_6}{K_4} > 0,$$

$$\omega_8 = \frac{(\varphi_{I2}K_4 + \varphi_{Q2}\eta_2)\omega_6}{\mu_H K_4} > 0. \tag{10}$$

Likewise, the components of the left eigenvector of $J(\xi_0)|_{\beta_{CV}=\beta_{CV}^*}$, $\mathbf{v} = (v_1, v_2, \ldots, v_8)$, satisfying $\mathbf{v}.\mathbf{w} = 1$ are

$$v_1 = v_2 = 0, \quad v_3 = v_3 > 0, \quad v_4 = v_5 = 0, \quad v_6 = v_6 > 0, \quad v_7 = v_8 = 0. \tag{11}$$

The associated bifurcation coefficients defined by a and b, given by:

$$a = \sum_{k,i,j=1}^{n} v_k \omega_i \omega_j \frac{\partial^2 f_k}{\partial x_i \partial x_j}(0,0) \quad \text{and} \quad b = \sum_{k,i=1}^{n} v_k \omega_i \frac{\partial^2 f_k}{\partial x_i \partial \beta_{CV}^*}(0,0),$$

are computed to be

$$a = -\frac{2\beta_{CV}^*(x_1^* v_3 + x_2^* v_6)}{N_H^{*2}}(\omega_3 + \omega_6)(\omega_1 + \omega_2 + \omega_3 + \omega_4\omega_5 + \omega_6 + \omega_7 + \omega_8)$$
$$+ \frac{2\beta_{CV}^*(\omega_3 + \omega_6)}{N^*}((\omega_1 + \psi_1\omega_5)v_3 + (\omega_2 + \psi_2\omega_8)v_6), \tag{12}$$

and

$$b = \sum_{k,i=1}^{20} v_k\omega_i \frac{\partial^2 f_k}{\partial x_i \partial \beta_{CV}^*}(0,0) = \frac{(\omega_3 + \omega_6)}{\mu_H + \theta_{CM}}(\mu_H v_3 + \theta_{CM} v_6) > 0. \qquad ∎$$

It is observed that the bifurcation coefficient b is positive. Hence, following from theorem 4.1 in Reference 50 we have that the model (1) exhibits backward bifurcation phenomenon if the backward bifurcation coefficient, a, given by (12) is positive. The associated backward bifurcation diagram is presented in Figure 2. It is imperative to note, that setting the COVID-19 reinfection terms $\psi_1 = \psi_2 = 0$ as well as the modification parameter for increased susceptibility to COVID-19 by comorbid susceptibles $\chi_{CM} = 0$, we observed that the bifurcation coefficient, $a < 0$. As a result, backward bifurcation does not occur in the COVID-19-comorbidity co-infection model, when there is no reinfection after recovery from COVID-19 and when appropriate measures are enforced to prevent comorbid-susceptible individuals from getting infected with COVID-19. This result is consistent with the result obtained in Section 3.3 above. The epidemiological interpretation is that if this phenomenon occurs, then the control of COVID-19 at the community level becomes difficult, even when the associated reproduction number $\mathcal{R}_{0C} < 1$.

3.5 | Global asymptotic stability of the CFE of the model

By removing the cause of the backward bifurcation in the model (1), that is, setting $\psi_1 = \psi_2 = \chi_{CM} = 0$, we have the following reduced model.

$$\frac{dS_H}{dt} = \Lambda_H - (\lambda_{CV} + \theta_{CM} + \mu_H)S_H,$$
$$\frac{dS_{CM}}{dt} = \theta_{CM}S_H - \mu_H S_{CM},$$
$$\frac{dI_{CV}}{dt} = \lambda_{CV}S_H - K_1 I_{CV},$$
$$\frac{dQ_{CV}}{dt} = \eta_1 I_{CV} - K_2 Q_{CV},$$
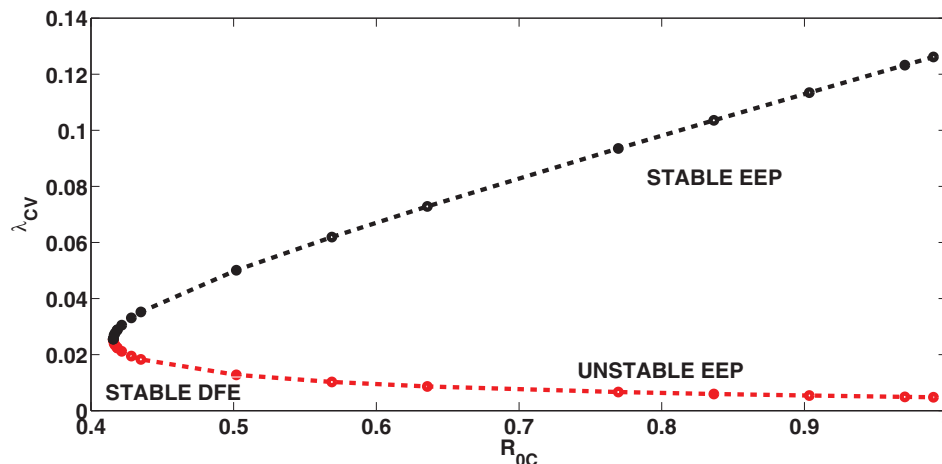$$\frac{dR_{CV}}{dt} = \varphi_{I1}I_{CV} + \varphi_{Q1}Q_{CV} - \mu_H R_{CV}, \tag{13}$$

FIGURE 2 Bifurcation diagram for the model (1). Parameter values used are: $\beta_{CV} = 0.148, \psi_1 = 25, \psi_2 = 40, \chi_{CM} = 1.2$. All other parameters as in Table 1 [Colour figure can be viewed at wileyonlinelibrary.com]

with

$$\lambda_{\text{CV}} = \frac{\beta_{\text{CV}} I_{\text{CV}}}{N_{\text{H}}}.$$

We can prove the global asymptotic stability of the CFE of the model (1).

Theorem 5. *Consider a special case of the model (1) (with $\psi_1 = \psi_2 = \chi_{\text{CM}} = 0$), given by (13). The CFE is GAS in $\mathcal{D}$ whenever $\overline{\mathcal{R}}_{0\text{C}} = \mathcal{R}_{0\text{C}}|_{\chi_{\text{CM}}=0} \leq 1$.*

Proof. We notice the compartments S_{cm}, Q_{cv}, and R_{cv}, do not impact the dynamics of COVID-19 in the considered epidemic model. Therefore, we continue our proof with the compartments S_h, and I_{cv}. For the rest of the proof, we consider the following Lyapunov function

$$\mathcal{L} = S_{\text{H}} - S_{\text{H}}^* - S_{\text{H}}^* \ln\left(\frac{S_{\text{H}}}{S_{\text{H}}^*}\right) + \frac{1}{2}I_{\text{CV}}^2. \tag{14}$$

Applying the derivative of the Lyapunov function (14) along the trajectories of the considered model, we have the following relationships

$$\begin{aligned}
\dot{\mathcal{L}} &= \left(1 - \frac{S_{\text{H}}^*}{S_{\text{H}}}\right)\frac{dS_{\text{H}}}{dt} + I_{\text{CV}}\frac{dI_{\text{CV}}}{dt}, \\
&= \left(1 - \frac{S_{\text{H}}^*}{S_{\text{H}}}\right)[\Lambda_{\text{H}} - (\lambda_{\text{CV}} + \theta_{\text{CM}} + \mu_{\text{H}})S_{\text{H}}] + I_{\text{CV}}[\lambda_{\text{CV}}S_{\text{H}} - K_1 I_{\text{CV}}], \\
&= \left(1 - \frac{S_{\text{H}}^*}{S_{\text{H}}}\right)[\Lambda_{\text{H}} - (\lambda_{\text{CV}} + \theta_{\text{CM}} + \mu_{\text{H}})S_{\text{H}}] + I_{\text{CV}}^2\left[\frac{\beta_{\text{CV}}S_{\text{H}}}{N_{\text{H}}} - K_1\right].
\end{aligned} \tag{15}$$

At CFE point ($\xi_0 = (S_{\text{H}}^*, S_{\text{CM}}^*, 0, 0, 0, 0, 0)$), we have the following form

$$\begin{aligned}
\dot{\mathcal{L}} &= -(\lambda_{\text{CV}} + \theta_{\text{CM}} + \mu_{\text{H}})\frac{(S_{\text{H}} - S_{\text{H}}^*)^2}{S_{\text{H}}} + I_{\text{CV}}^2\left[\frac{\beta_{\text{CV}}S_{\text{H}}^*}{N_{\text{H}}^*} - K_1\right], \\
&\leq -(\lambda_{\text{CV}} + \theta_{\text{CM}} + \mu_{\text{H}})\frac{(S_{\text{H}} - S_{\text{H}}^*)^2}{S_{\text{H}}} + \frac{I_{\text{CV}}^2}{K_1}(\overline{\mathcal{R}}_{0\text{C}} - 1).
\end{aligned} \tag{16}$$

∎

Hence, $\mathcal{L} < 0$ if and only if $\overline{\mathcal{R}}_{0\text{C}} \leq 1$. Therefore, $\mathcal{L}$ is a Lyapunov function for the system (13). It follows by the La Salle's Invariance Principle,[51] that the CFE of the model (13) is globally asymptotically stable whenever $\overline{\mathcal{R}}_{0\text{C}} \leq 1$.

4 | NUMERICAL SIMULATIONS

In this section, simulations of the model are carried out to assess the impact of various control strategies on the dynamics of COVID-19 and comorbidity co-infection. The equations of the model (1) are solved numerically using the MATLAB ode45 solver which is based on the fourth-order Runge–Kutta method. We shall also estimate some of the key parameters of the model and initial conditions before the simulations.

4.1 | Model fitting and estimation of parameters and initial conditions

The population of Lagos is approximately estimated at 14,368,332.[52] Also, based on a study carried out by Dahiru et al.[18] on the prevalence of DM in Lagos, Nigeria and since the first COVID-19 case in Lagos (with no evidence of comorbidity) was announced on March 16, 2020, we set our initial conditions to be $S_h(0) = 0.93 \times 14,368,332$, $S_{cm}(0) = 0.07 \times 14,368,332$, $Q_{cv}(0) = 1$, $R_{cv}(0) = 0$, $Q_{cvcm} = 0$, $R_{cm}(0) = 0$.

Two optimization algorithms were combined for data fitting, a genetic algorithm (GA) algorithm and the *fmincon*algorithm[44,53] in MATLAB to estimate the values of the effective contact rate for COVID-19 transmission, β_{CV}, the

case detection rates for singly infected and co-infected individuals, η_1 and η_2, respectively, the comorbidity induced death rate for co-infected individuals, δ_2 and the COVID-19 re-infection rates ψ_1 and ψ_2 for singly and co-infected individuals respectively. We equally estimated the initial conditions $I_{cv}(0)$ and $I_{cvcm}(0)$. All the estimates were done using the daily confirmed and active cases for Lagos, Nigeria, from March 16, 2020 to June 24, 2020.[54] Table 2 gives the estimated values of $\beta_{CV}, \eta_1, \eta_2, \delta_2, \psi_1,$ and ψ_2, and the initial conditions $I_{cv}(0)$ and $I_{cvcm}(0)$, together with the calculated reproduction number (R_{0i}).

4.2 | Discussion of results

Figure 3 presents the fitting of the model when the cumulative active cases were used to fit the model. The figure showed that the co-infection model (1) fitted well to the Lagos COVID-19 data (daily cumulative active cases).

As observed in Figure 4, the projection is made for the cumulative number of active cases using the developed model. It is observed that the cumulative active cases (including those with comorbidity) peaked at 130,000 cases in about 180 days

Parameter	Baseline value	Range	Reference
μ_H	0.0000491 /day		55
Λ_H	705 /day		52,55
β_{CV}	0.2001	[0.1, 0.3]	Fitted
$\varphi_{i1}, \varphi_{i2}$	0.13978 /day	$[\frac{1}{30}, \frac{1}{3}]$/day	11
$\varphi_{q1}, \varphi_{q1}$	$\frac{1}{15}$ /day	$[\frac{1}{30}, \frac{1}{3}]$/day	Estimated from Reference 56
δ_1	0.015 /day	[0.001, 0.1]	42
η_1	0.0059 /day	[0.001,0.05]	Fitted
η_2	0.0895 /day	[0.001,0.05]	Fitted
θ_{CM}	0.0000034294	[0.0000001,0.00001]	Fitted
ψ_1	0.0013	[0.001,0.005]	Fitted
ψ_2	0.0013	[0.001,0.005]	Fitted
χ_{CM}	1.2	[1,3]	Inferred from Reference 13
δ_2	0.0500	[0.01,0.08]	Fitted
$I_{cv}(0)$	135	[100,400]	Fitted
$I_{cvcm}(0)$	21	[20,50]	Fitted
$\mathcal{R}_{0C}$	1.3423		

TABLE 2 Estimated parameters and variables when the model 1 was fitted using the cumulative number of confirmed and active cases. The estimates were from the "best fit"
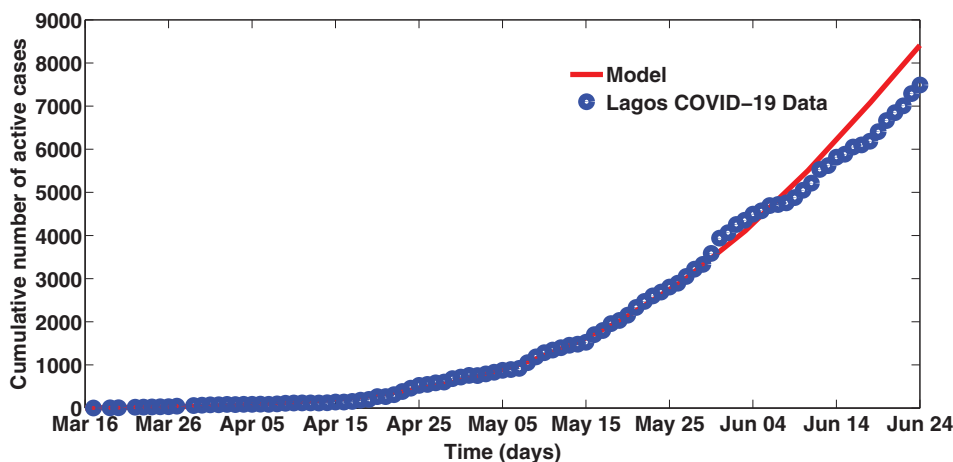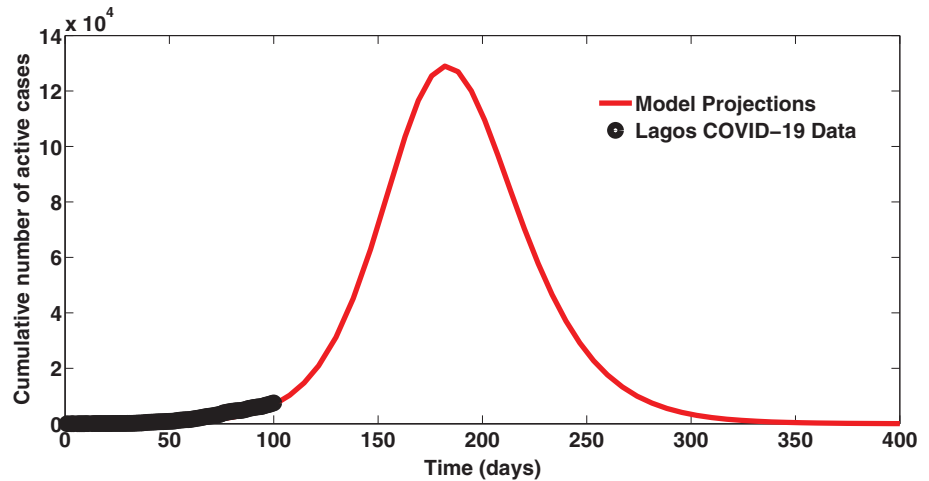

FIGURE 3 Fitting the cumulative number of active cases [Colour figure can be viewed at wileyonlinelibrary.com]

FIGURE 4 Projections for the cumulative number of active cases [Colour figure can be viewed at wileyonlinelibrary.com]

(counting from March 16, 2020). Figure 5 presents the simulations of the cumulative number of active cases (including those with comorbidity) at different levels of susceptibility of comorbid susceptibles ($0.2 \leq \chi_{CM} \leq 1.2$). It is observed that the peak value attained at different levels and reduces with decreasing value of the modification parameter χ_{CM}. We notice that as preventive measures such as social distancing, use of face mask in public places are enforced to reduce the probability of infection by comorbid susceptibles, the infection peaks reduce steadily. Similar conclusions are reached when the cumulative number of active cases (without comorbidity) are simulated, as seen in Figure 6. The simulations of the cumulative number of active cases (including those with comorbidity), at different reinfection rates, depicted in Figure 7 shows the attainment of infections peaks around 200 days (counting from March 16, 2020), although infection peak reduces with decreasing reinfection of those who have recovered from a previous COVID-19 infection. Figure 8 is interpreted in a similar manner.

The contour plot of the reproduction number $\mathcal{R}_{0C}$ with detection rate for singly infected individuals (η_1) and detection rate for co-infected individuals (η_2), shown in Figure 9(A), reveal that if the detection rate for infected individuals co-infected with comorbidity can be increased to about 0.7 per day and the detection rate for infected individuals (without comorbidites) kept at 0.3 per day, then the reproduction number $\mathcal{R}_{0C}$ can be brought below unity and COVID-19

FIGURE 5 Simulations of the Cumulative number of active cases (including those with comorbidity): effect of χ_{CM} [Colour figure can be viewed at wileyonlinelibrary.com]
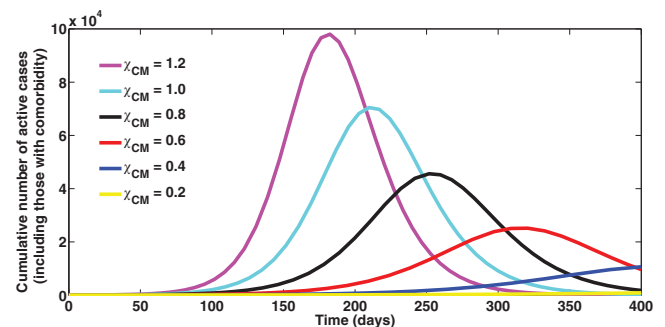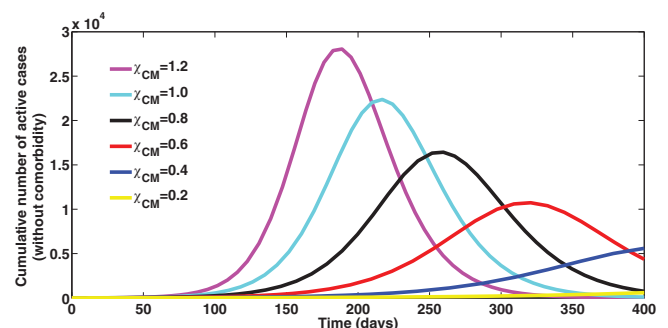

FIGURE 6 Simulations of the Cumulative number of active cases (without comorbidity): effect of χ_{CM} [Colour figure can be viewed at wileyonlinelibrary.com]
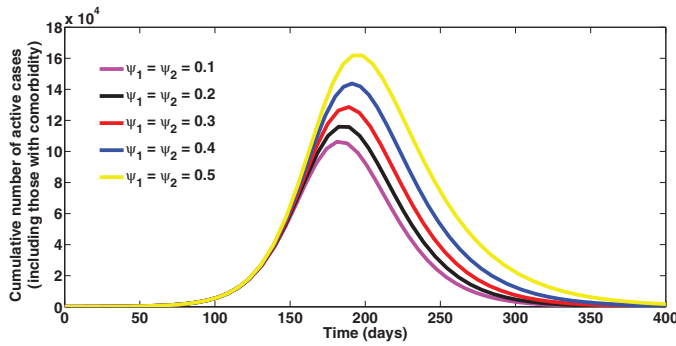
FIGURE 7 Simulations of the Cumulative number of active cases (including those with comorbidity): effect of ψ_1 and ψ_2 [Colour figure can be viewed at wileyonlinelibrary.com]
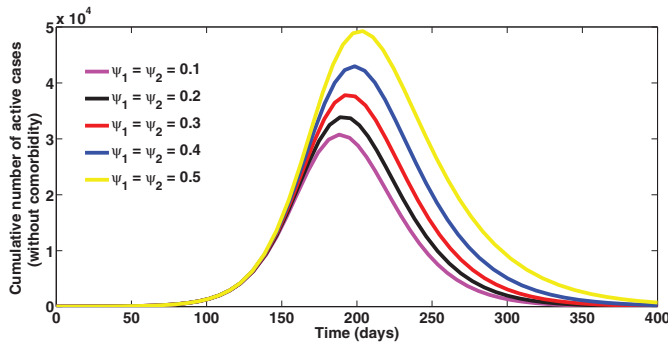

FIGURE 8 Simulations of the Cumulative number of active cases (without comorbidity): effect of ψ_1 and ψ_2 [Colour figure can be viewed at wileyonlinelibrary.com]
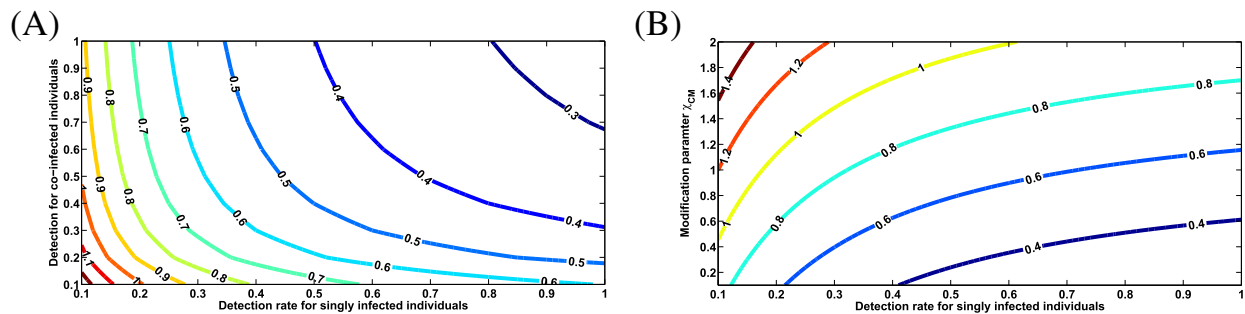

FIGURE 9 Contour plots of $\mathcal{R}_{0C}$. Here, $\beta_{CV} = 0.2001, \psi_1 = \psi_2 = 0.4$. All other parameters as in Table 1. (A) A contour plot of $\mathcal{R}_{0C}$ as a function of detection rate for singly infected individuals (η_1) and detection rate for co-infected individuals (η_2). (B) A contour plot of $\mathcal{R}_{0C}$ as a function of detection rate for singly infected individuals (η_1 and the modification parameter for high susceptibility of those with comorbidity χ_{CM}) [Colour figure can be viewed at wileyonlinelibrary.com]

infection eliminated from the population. The contour plot of the reproduction number, $\mathcal{R}_{0C}$, as a function of detection rate for singly infected individuals (η_1) and the modification parameter for high susceptibility of comorbid susceptibles, depicted in Figure 9(B) shows that if policies are strictly put in place to step down the probability of COVID-19 infection by comorbid susceptibles to as low as 0.4 per day and step up the detection rate for singly infected individuals to 0.7 per day, then the reproduction number can be brought very low below one, and COVID-19 infection eliminated from the population.

5 | ANALYSIS OF THE OPTIMAL CONTROL MODEL

The Pontryagin's Maximum Principle shall be applied, in this section, to determine the necessary conditions for the optimal control of the model. We incorporate time-dependent controls into the model (1) to determine the optimal strategy for controlling the spread of COVID-19. Thus, we have,

$$\frac{dS_H}{dt} = \Lambda_H - (\lambda_{CV} + \theta_{CM} + \mu_H)S_H,$$

$$\frac{dS_{HCM}}{dt} = \theta_{CM}S_H - (1 - u_1)\chi_{CM}\lambda_{CV}S_{HCM} - \mu_H S_{HCM},$$

$$\frac{dI_{CV}}{dt} = \lambda_{CV}S_H - ((1 + u_2)\eta_1 + \varphi_{I1} + \mu_H)I_{CV} + (1 - u_3)\psi_1\lambda_{CV}R_{CV},$$

$$\frac{dQ_{CV}}{dt} = (1 + u_2)\eta_1 I_{CV} - (\varphi_{Q1} + \delta_1 + \mu_H)Q_{CV},$$

$$\frac{dR_{CV}}{dt} = \varphi_{I1}I_{CV} + \varphi_{Q1}Q_{CV} - \mu_H R_{CV} - (1 - u_3)\psi_1\lambda_{CV}R_{CV},$$

$$\frac{dI_{CVCM}}{dt} = (1 - u_1)\chi_{CM}\lambda_{CV}S_{HCM} - ((1 + u_2)\eta_2 + \varphi_{I2} + \mu_H)I_{CVCM} + (1 - u_3)\psi_2\lambda_{CV}R_{CM},$$

$$\frac{dQ_{CVCM}}{dt} = (1 + u_2)\eta_2 I_{CVCM} - (\delta_1 + \delta_2 + \varphi_{Q2} + \mu_H)Q_{CVCM},$$

$$\frac{dR_{CM}}{dt} = \varphi_{I2}I_{CVCM} + \varphi_{Q2}Q_{CVCM} - \mu_H R_{CM} - (1 - u_3)\psi_2\lambda_{CV}R_{CM}, \tag{17}$$

subject to the initial conditions

$S_H(0) = S_H^0, S_{HCM}(0) = S_{HCM}^0, I_{CV}(0) = I_{CV}^0, Q_{CV}(0) = Q_{CV}^0, R_{CV}(0) = R_{CV}^0, I_{CVCM}(0) = I_{CVCM}^0, Q_{CVCM}(0) = Q_{CVCM}^0, R_{CM}(0) = R_{CM}^0$, with

$$\lambda_{CV} = \frac{\beta_{CV}(I_{CV} + I_{CVCM})}{N_H}.$$

The control functions, $u_1(t), u_2(t)$, and $u_3(t)$ are bounded, Lebesgue integrable functions. The control $u_1(t)$ represents the efforts geared towards preventing incident COVID-19 infections by comorbid susceptible humans. The control $u_2(t)$ is COVID-19 detection control that represents the fraction of active individuals that are identified and quarantined in an isolation centre for effective treatment and prevention of contacts with susceptible individuals; therefore the term $1 + u_2(t)$ will denote the effort that sustains the quarantine policy which "holds down" the quarantined for proper and effective treatment. Efforts aimed at preventing reinfection by those who have fully recovered from COVID-19 is represented by $u_3(t)$. The control u_1 satisfies $0 \leq u_1 \leq 0.9$, the controls u_2 and u_3 satisfy $0 < u_2, u_3 \leq 1$. The optimal control system examines scenarios where the number of infectious cases and the cost of implementing the controls $u_1(t), u_2(t)$, and $u_3(t)$ are minimized subject to the state system (17). For this, we consider the objective functional

$$J[u_1, u_2, u_3] = \int_0^T \left[I_{CV}(t) + I_{CVCM}(t) + \frac{B_1}{2}u_1^2 + \frac{B_2}{2}u_2^2 + \frac{B_3}{2}u_3^2 \right] dt, \tag{18}$$

T is the final time. We seek to find an optimal control, u_1^*, u_2^*, u_3^*, such that

$$J(u_1^*, u_2^*, u_3^*) = min\{J(u_1^*, u_2^*, u_3^*) | u_1, u_2, u_3 \in U\}, \tag{19}$$

where $U = \{(u_1^*, u_2^*, u_3^*)\}$ such that u_1^*, u_2^*, u_3^* are measurable with $0 \leq u_1^* \leq 0.9, 0 \leq u_2^* \leq 1, 0 \leq u_3^* \leq 1$, for $t \in [0, T]$ is the control set. The Pontryagin's Maximum Principle[57] gives the necessary conditions which an optimal control pair must satisfy. This principle transforms (17), (18) and (19) into a problem of minimizing a Hamiltonian, $\mathcal{H}$, pointwisely with regards to the control functions, u_1, u_2, u_3:

$$\mathcal{H} = I_{CV}(t) + I_{CVCM}(t) + \frac{B_1}{2}u_1^2 + \frac{B_2}{2}u_2^2 + \frac{B_3}{2}u_3^2$$

$$+ \lambda_{S_H}[\Lambda_H - (\lambda_{CV} + \theta_{CM} + \mu_H)S_H]$$

$$+ \lambda_{S_{HCM}}[\theta_{CM}S_H - (1 - u_1)\chi_{CM}\lambda_{CV}S_{HCM} - \mu_H S_{HCM}]$$

$$+ \lambda_{I_{CV}}[\lambda_{CV}S_H - ((1 + u_2)\eta_1 + \varphi_{I1} + \mu_H)I_{CV} + (1 - u_3)\psi_1\lambda_{CV}R_{CV}]$$

$$+ \lambda_{Q_{CV}}[(1 + u_2)\eta_1 I_{CV} - (\varphi_{Q1} + \delta_1 + \mu_H)Q_{CV}]$$

$$+ \lambda_{R_{CV}}[\varphi_{I1}I_{CV} + \varphi_{Q1}Q_{CV} - \mu_H R_{CV} - (1 - u_3)\psi_1\lambda_{CV}R_{CV}]$$

$$+ \lambda_{I_{\text{CVCM}}}[(1 - u_1)\chi_{\text{CM}}\lambda_{\text{CV}}S_{\text{HCM}} - ((1 + u_2)\eta_2 + \varphi_{I2} + \mu_{\text{H}})I_{\text{CVCM}} + (1 - u_3)\psi_2\lambda_{\text{CV}}R_{\text{CM}}]$$

$$+ \lambda_{Q_{\text{CVCM}}}[(1 + u_2)\eta_2 I_{\text{CVCM}} - (\delta_1 + \delta_2 + \varphi_{Q2} + \mu_{\text{H}})Q_{\text{CVCM}}]$$

$$+ \lambda_{R_{\text{CM}}}[\varphi_{I2}I_{\text{CVCM}} + \varphi_{Q2}Q_{\text{CVCM}} - \mu_{\text{H}}R_{\text{CM}} - (1 - u_3)\psi_2\lambda_{\text{CV}}R_{\text{CM}}]. \tag{20}$$

Theorem 6. *For an optimal control set u_1, u_2, u_3 that minimizes J over U, there are adjoint variables, $\lambda_1, \lambda_2, \ldots, \lambda_8$ satisfying*

$$-\frac{\partial \lambda_i}{\partial t} = \frac{\partial \mathcal{H}}{\partial i},$$

and with transversality conditions

$$\lambda_i(t_f) = 0, \qquad where, \quad i = S_{\text{H}}, S_{\text{HCM}}, I_{\text{CV}}, Q_{\text{CV}}, R_{\text{CV}}, I_{\text{CVCM}}, Q_{\text{CVCM}}, R_{\text{CM}}. \tag{21}$$

Furthermore,

$$u_1^* = \max\left\{0, \min\left(1, \frac{(\lambda_6 - \lambda_2)\beta_{\text{CV}}\chi_{\text{CM}}S_{\text{CM}}(I_{\text{CV}} + I_{\text{CVCM}})}{B_1 N_{\text{H}}}\right)\right\},$$

$$u_2^* = \max\left\{0, \min\left(1, \frac{(\lambda_3 - \lambda_4)I_{\text{CV}}\eta_1 + (\lambda_6 - \lambda_7)I_{\text{CVCM}}\eta_2}{B_2}\right)\right\},$$

$$u_3^* = \max\left\{0, \min\left(1, \frac{(\lambda_3 - \lambda_5)\beta_{\text{CV}}R_{\text{CV}}(I_{\text{CV}} + I_{\text{CVCM}}) + (\lambda_6 - \lambda_8)\beta_{\text{CV}}R_{\text{CM}}(I_{\text{CV}} + I_{\text{CVCM}})}{B_3 N_{\text{H}}}\right)\right\}. \tag{22}$$

Proof of Theorem 6. Suppose $U^* = (u_1^*, u_2^*, u_3^*)$ is an optimal control and $S_{\text{H}}^*, S_{\text{HCM}}^*, I_{\text{CV}}^*, Q_{\text{CV}}^*, R_{\text{CV}}^*, I_{\text{CVCM}}^*, Q_{\text{CVCM}}^*, R_{\text{CM}}^*$ are the corresponding state solutions. Applying the Pontryagin's Maximum Principle,[57] there exist adjoint variables satisfying:

$$-\frac{d\lambda_{S_{\text{H}}}}{dt} = \frac{\partial \mathcal{H}}{\partial S_{\text{H}}}, \quad \lambda_{S_{\text{H}}}(t_f) = 0, \quad -\frac{d\lambda_{S_{\text{HCM}}}}{dt} = \frac{\partial \mathcal{H}}{\partial S_{\text{HCM}}}, \quad \lambda_{S_{\text{HCM}}}(t_f) = 0, \quad -\frac{d\lambda_{I_{\text{CV}}}}{dt} = \frac{\partial \mathcal{H}}{\partial I_{\text{CV}}}, \quad \lambda_{I_{\text{CV}}}(t_f) = 0,$$

$$-\frac{d\lambda_{Q_{\text{CV}}}}{dt} = \frac{\partial \mathcal{H}}{\partial Q_{\text{CV}}}, \quad \lambda_{Q_{\text{CV}}}(t_f) = 0, -\frac{d\lambda_{R_{\text{CV}}}}{dt} = \frac{\partial \mathcal{H}}{\partial R_{\text{CV}}}, \quad \lambda_{R_{\text{CV}}}(t_f) = 0, \quad -\frac{d\lambda_{I_{\text{CVCM}}}}{dt} = \frac{\partial \mathcal{H}}{\partial I_{\text{CVCM}}}, \quad \lambda_{I_{\text{CVCM}}}(t_f) = 0, \tag{23}$$

with transversality conditions;

$\lambda_{S_{\text{H}}}(t_f) = \lambda_{S_{\text{HCM}}}(t_f) = \lambda_{I_{\text{CV}}}(t_f) = \lambda_{Q_{\text{CV}}}(t_f) = \lambda_{R_{\text{CV}}}(t_f) = \lambda_{I_{\text{CVCM}}}(t_f) = \lambda_{Q_{\text{CVCM}}}(t_f) = \lambda_{R_{\text{CM}}}(t_f) = 0.$ We can determine the behaviour of the control by differentiating the Hamiltonian, $\mathcal{H}$ with respect to the controls(u_1, u_2, u_3) at t. On the interior of the control set, where $0 < u_j < 1$ for all ($j = 1, 2, 3$), we obtain

$$0 = \frac{\partial \mathcal{H}}{\partial u_1} = B_1 N_{\text{H}} u_1^* + (\lambda_2 - \lambda_6)\beta_{\text{CV}}\chi_{\text{CM}}S_{\text{CM}}(I_{\text{CV}} + I_{\text{CVCM}}),$$

$$0 = \frac{\partial \mathcal{H}}{\partial u_2} = B_2 u_2^* + (\lambda_4 - \lambda_3)\eta_1 I_{\text{CV}} + (\lambda_7 - \lambda_6)\eta_2 I_{\text{CVCM}},$$

$$0 = \frac{\partial \mathcal{H}}{\partial u_3} = B_3 N_{\text{H}} u_3^* + \beta_{\text{CV}}(I_{\text{CV}} + I_{\text{CVCM}})R_{\text{CV}}(\lambda_5 - \lambda_3) + \beta_{\text{CV}}(I_{\text{CV}} + I_{\text{CVCM}})R_{\text{CM}}(\lambda_8 - \lambda_6). \tag{24}$$

∎

Therefore, we have that

$$u_1^* = \frac{(\lambda_6 - \lambda_2)\beta_{\text{CV}}\chi_{\text{CM}}S_{\text{CM}}(I_{\text{CV}} + I_{\text{CVCM}})}{B_1 N_{\text{H}}},$$

$$u_2^* = \frac{(\lambda_3 - \lambda_4)I_{\text{CV}}\eta_1 + (\lambda_6 - \lambda_7)I_{\text{CVCM}}\eta_2}{B_2},$$

$$u_3^* = \frac{(\lambda_3 - \lambda_5)\beta_{\text{CV}}R_{\text{CV}}(I_{\text{CV}} + I_{\text{CVCM}}) + (\lambda_6 - \lambda_8)\beta_{\text{CV}}R_{\text{CM}}(I_{\text{CV}} + I_{\text{CVCM}})}{B_3 N_{\text{H}}}. \tag{25}$$

$$u_1^* = \max\left\{0, \min\left(1, \frac{(\lambda_6 - \lambda_2)\beta_{CV}\chi_{CM}S_{CM}(I_{CV} + I_{CVCM})}{B_1 N_H}\right)\right\},$$

$$u_2^* = \max\left\{0, \min\left(1, \frac{(\lambda_3 - \lambda_4)I_{CV}\eta_1 + (\lambda_6 - \lambda_7)I_{CVCM}\eta_2}{B_2}\right)\right\},$$

$$u_3^* = \max\left\{0, \min\left(1, \frac{(\lambda_3 - \lambda_5)\beta_{CV}R_{CV}(I_{CV} + I_{CVCM}) + (\lambda_6 - \lambda_8)\beta_{CV}R_{CM}(I_{CV} + I_{CVCM})}{B_3 N_H}\right)\right\}. \tag{26}$$

5.1 | Strategy A: COVID-19 prevention among Comorbid susceptibles ($u_1 \neq 0$)

Simulations of the optimal control system when the strategy that prevents COVID-19 among comorbid susceptibles ($u_1 \neq 0$) is implemented, are presented in Figure 10. It is seen that when this intervention strategy is implemented, there is a significant decrease in the total number of individuals singly infected with COVID-19 (Figure 10(A)) and those co-infected with COVID-19 and comorbidity (Figure 10 (B)). Specifically, this strategy averts 354,600 new cases of COVID-19 and also prevents 35,297 new cases of co-infection of COVID-19 and comorbidity after 200 days. The control profile for this control strategy given in Figure 11 shows that control u_1 rises steadily to its peak in about 160 days, and then drops to zero at time $t = 200$ days.

5.2 | Strategy B: Case detection control ($u_2 \neq 0$)

Simulations of the optimal control system when the case detection control ($u_2 \neq 0$) is implemented, are presented in Figure 12. It is seen that when this intervention strategy is implemented, there is a significant drop in the total number
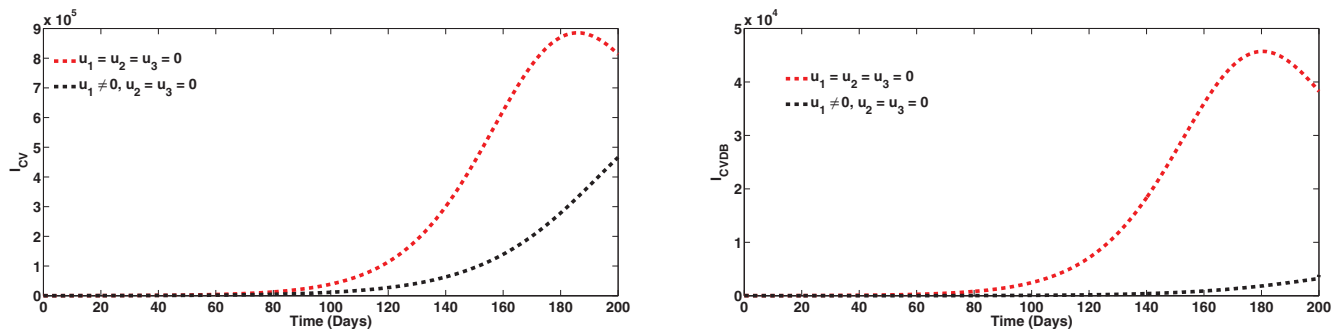

FIGURE 10 Plots of the total number of COVID-19-infected individuals when strategy A is implemented ($u_1 \neq 0$). Here, $\beta_{CV} = 0.2001, \psi_1 = \psi_2 = 0.4$. All other parameters as in Table 1 [Colour figure can be viewed at wileyonlinelibrary.com]
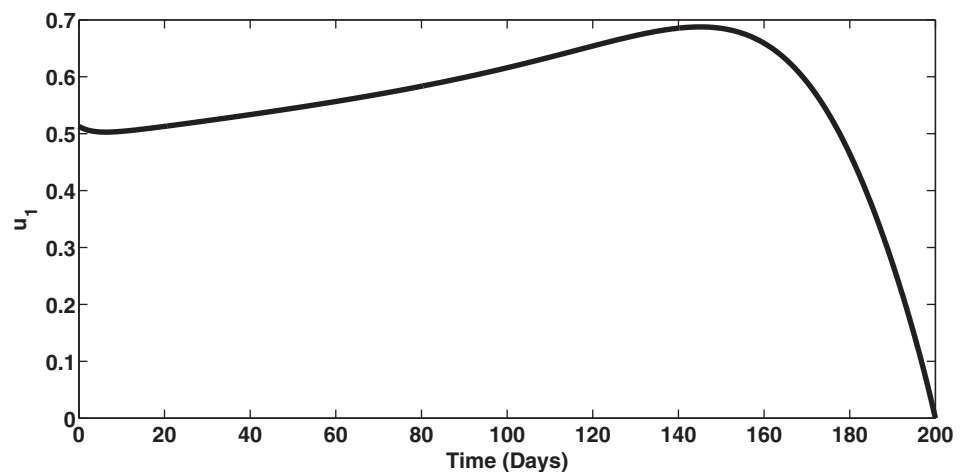

FIGURE 11 Control profile for the effect of the control u_1 on the dynamics of the model (1). Here, $\beta_{CV} = 0.2001, \psi_1 = \psi_2 = 0.4$. All other parameters as in Table 1
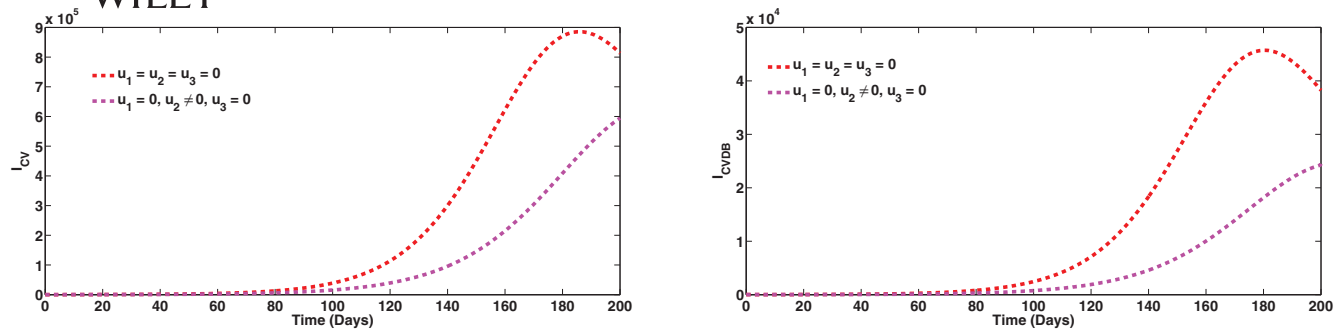
FIGURE 12 Plots of the total number of COVID-19-infected individuals when strategy B is implemented ($u_2 \neq 0$). Here, $\beta_{CV} = 0.2001, \psi_1 = \psi_2 = 0.4$. All other parameters as in Table 1 [Colour figure can be viewed at wileyonlinelibrary.com]

of individuals singly infected with COVID-19 and the co-infection cases. To be specific, this strategy averts 225,800 new COVID-19 cases after 200 days. The strategy also averts 14,020 new co-infection cases after 200 days. The control profile for this intervention control given in Figure 13 also shows that control u_2 drops for the first 10 days and then rises steadily till about 160 days before falling down at time $t = 200$ days.

5.3 | Strategy C: Control against COVID-19 reinfection ($u_3 \neq 0$)

Simulations of the optimal control system when control against COVID-19 reinfection ($u_3 \neq 0$) is implemented, are presented in Figure 14. It is observed that when this intervention strategy is applied, there is a significant reduction in the
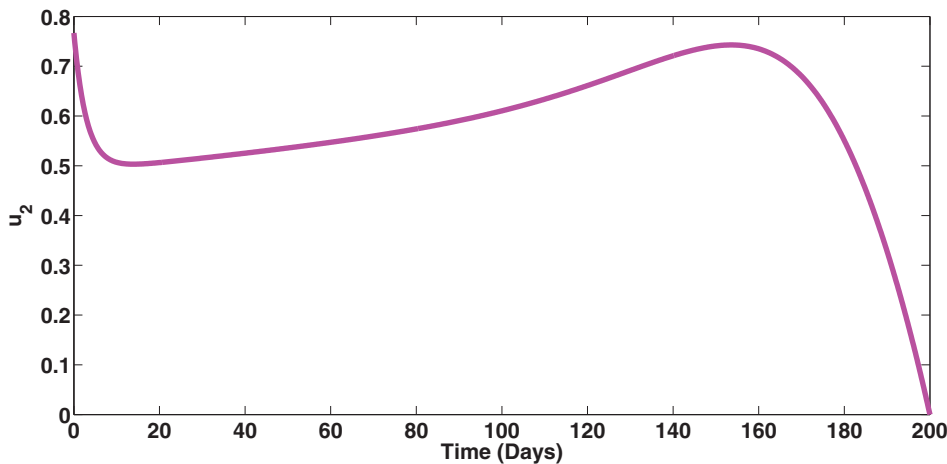

FIGURE 13 Control profile for the effect of the control u_2 on the dynamics of the model (1). Here, $\beta_{CV} = 0.2001$, $\psi_1 = \psi_2 = 0.4$. All other parameters as in Table 1 [Colour figure can be viewed at wileyonlinelibrary.com]
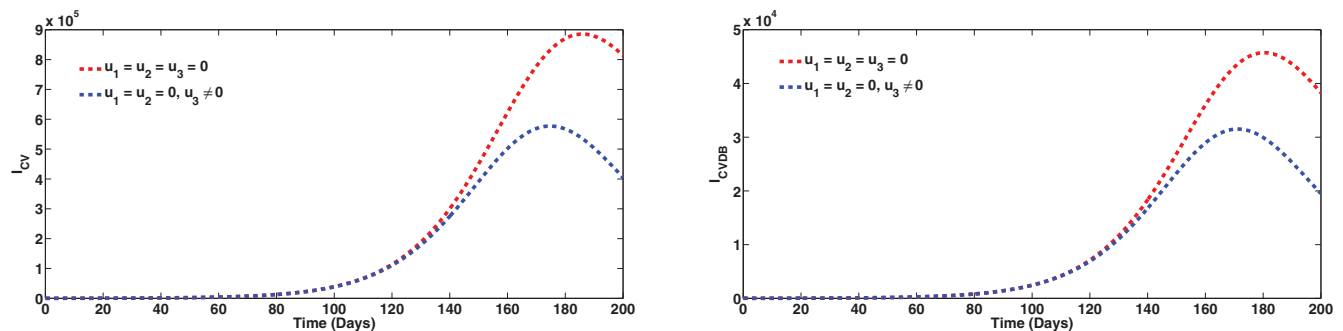

FIGURE 14 Plots of the total number of COVID-19-infected individuals when strategy C is implemented ($u_3 \neq 0$). Here, $\beta_{CV} = 0.2001$, $\psi_1 = \psi_2 = 0.4$. All other parameters as in Table 1 [Colour figure can be viewed at wileyonlinelibrary.com]

total number of individuals singly infected with COVID-19 and those co-infected with comorbidity. As a matter of fact, this strategy averts 411,500 new COVID-19 cases and 18,430 co-infection new cases. The control profile for this intervention control given in Figure 15 shows that control u_3 rises steadily to its maximum value in about 50 days and maintains this peak for the entire period of the simulation.

5.4 | Cost-effectiveness analysis

In this section, we seek to determine the most cost-effective intervention strategy in combating COVID-19 and comorbidity co-infection. To achieve this, two methods are employed: the average cost-effectiveness ratio (ACER) and the incremental cost-effectiveness ratio (ICER). The cost-effectiveness analysis is used to evaluate the health interventions related benefits so as to justify the costs of the strategies.[58] This is obtained by comparing the differences among the health outcomes and costs of those interventions. ACER deals with a single intervention strategy and weighing the intervention against its baseline option. It is the ratio of the total cost of the intervention to the total number of infection averted by the intervention. The formula is given thus:

$$ACER = \frac{\text{Total cost produced by intervention}}{\text{Total number of infection averted}}.$$

Likewise, ICER is concerned with the comparison of the differences between the costs and health outcomes of two alternative intervention strategies competing for the same resources. It is the ratio of the change in costs of two alternative strategies to the change in the total number of infection averted by the two strategies. The ICER formula is given by:

$$ICER = \frac{\text{Difference in costs between strategies}}{\text{Difference in health effects between strategies}}.$$

We calculated the total number of cases averted and the total cost of the strategies applied in Table 3. The total number of cases prevented is obtained by calculating the total number of individuals when controls are implemented and the total number when control is not administered. In a similar manner, we apply the cost functions $\frac{1}{2}B_1u_1^2, \frac{1}{2}B_2u_2^2, \frac{1}{2}B_3u_3^2$, over time, to compute the total cost for the various strategies that were carried out. We assume the weight constants $B_1 = 400$, $B_3 = 500$ while $B_2 = 700$. We assumed here that, the cost of implementing the case detection control is much higher compared to the cost of implementing the preventive controls (which are mainly nonpharmaceutical). The cost-effectiveness of strategy B (case detection control) and strategy A (COVID-19 prevention among Comorbid susceptibles ($u_1 \neq 0$)) are now compared.

$$ICER (B) = \frac{700}{239,820} = 0.002919$$

$$ICER (A) = \frac{400 - 700}{389,897 - 239,820} = -0.001999$$
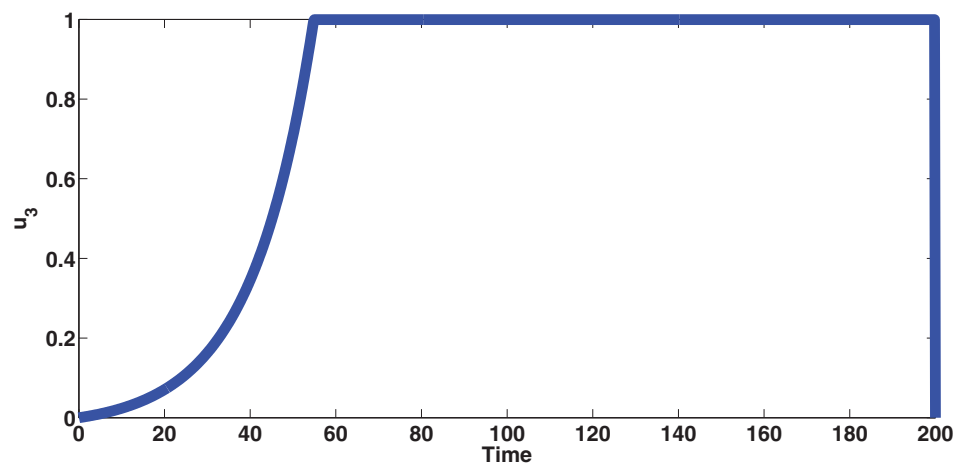

FIGURE 15 Control profile for the effect of the control u_3 on the dynamics of the model (1). Here, $\beta_{CV} = 0.2001$, $\psi_1 = \psi_2 = 0.4$. All other parameters as in Table 1 [Colour figure can be viewed at wileyonlinelibrary.com]

Strategy	Total infection averted	Total cost	ACER	ICER
B: $u_2(t)$	239,820	700	0.002919	0.002919
A: $u_1(t)$	389,897	400	0.001026	−0.001999
C: $u_3(t)$	429,930	500	0.001163	0.002498

TABLE 3 Increasing order of the total infection averted due to the control strategies

Abbreviations: ACER, average cost-effectiveness ratio; ICER, incremental cost-effectiveness ratio.

Strategy	Total infection averted	Total cost	ACER	ICER
A: $u_1(t)$	389,897	400	0.001026	0.001026
C: $u_3(t)$	429,930	500	0.001163	0.002498

TABLE 4 Increasing order of the total infection averted due to the control strategies

Abbreviations: ACER, average cost-effectiveness ratio; ICER, incremental cost-effectiveness ratio.

From the computations of ICER (B) and ICER(A), we observe that ICER (B) is greater than ICER (A), showing that strategy B is more costly and less effective compared to strategy A. Therefore, strategy B is removed from subsequent ICER computations, shown in Table 4. We shall now compare strategies A and C.

Comparing strategy A (control against COVID-19 infection by comorbid susceptibles) and strategy C (control against COVID-19 re-infection), we observe that ICER (C) is greater than ICER (A), showing that strategy C is more expensive and less effective compared to strategy A. Consequently, strategy A (the strategy that prevents COVID-19 infection by comorbid susceptibles) has the least ICER and is the most cost-effective of all the control strategies for the prevention of COVID-19. This also conforms with the results obtained from ACER method in Table 3 that strategy A is the most cost-effective strategy.

$$\text{ICER (A)} = \frac{400}{389,897} = 0.001026$$

$$\text{ICER (C)} = \frac{500 - 400}{429,930 - 389,897} = 0.002498$$

6 | CONCLUSION

In this work, we developed and analyzed a mathematical model for the dynamics of COVID-19 infection in order to assess the impacts of prior comorbidity on COVID-19 complications and COVID-19 reinfection. The model was simulated using data relevant to the dynamics of the diseases in Lagos, Nigeria, making predictions for the attainment of peak periods in the presence or absence of comorbidity. The model was shown to undergo the phenomenon of backward bifurcation which was caused by the parameter accounting for increased susceptibility to COVID-19 infection by comorbid susceptibles as well as the rate of reinfection by those who have recovered from a previous COVID-19 infection. The epidemiological interpretation of this phenomenon is that if recovery from COVID-19 does not confer lifelong immunity and efforts are not put in place to prevent COVID-19 infections by comorbid susceptible individuals, then the control of COVID-19 becomes difficult in the population, even when the associated reproduction number $\mathcal{R}_{0C} < 1$. Hence, it is recommended that efforts should be made by those in authority and policy makers to recommend preventive measures to curb COVID-19 infection by comorbid susceptibles and reinfection with COVID-19 so as to bring the burden of COVID-19 infection very low at the community level.

Sensitivity analysis of the model when the population of individuals co-infected with COVID-19 and comorbidity is used as response function revealed that the top ranked parameters that drive the dynamics of the co-infection model are the effective contact rate for COVID-19 transmission, β_{CV}, the parameter accounting for increased susceptibility to COVID-19 by comorbid susceptibles, χ_{CM}, the comorbidity development rate, θ_{CM}, the detection rate for singly infected and co-infected individuals, η_1 and η_2, as well as the recovery rate from COVID-19 for co-infected individuals, φ_{i2}. Simulations of the cumulative number of active cases (including those with comorbidity), at different reinfection rates, show infection peaks reducing with decreasing reinfection of those who have recovered from a previous COVID-19 infection. Optimal control and cost effectiveness analysis of the model reveals that the strategy that prevents

COVID-19 infection by comorbid susceptibles is the most cost-effective of all the control strategies for the prevention of COVID-19 infections.

The authors in References 44 and 46 both pointed to the importance of facemask usage, case detection and social distancing as effective measures in combating COVID-19 infections. In addition, the authors in Reference 45 showed the strategy which involves cleaning of environmental surfaces with home-based detergents is the most cost-effective strategy in the control of COVID-19 infection. However, results from the current study has shown that if efforts are not put in place to avert reinfection by those who have recovered from previous COVID-19 infection and also to prevent COVID-19 infections by comorbid susceptible individuals, then the control of the disease will become very difficult.

This study can be extended in numerous ways, including incorporating the dynamics of two-strain COVID-19 co-infection with other comorbidities and by considering COVID-19 vaccination model. Also, the current model can be analyzed using fractional derivatives. Further studies may also consider stochastic version of the co-infection model.

CONFLICT OF INTEREST

The authors declare that they have no conflict of interests.

DATA AVAILABILITY STATEMENT

The data that support the findings of this study are available from the corresponding author upon reasonable request.

ORCID

Andrew Omame https://orcid.org/0000-0002-1252-1650

REFERENCES

1. Lai C-C, Wang C-Y, Hsueh P-R. Co-infections among patients with COVID-19: the need for combination therapy with non-anti-SARS-CoV-2 agents. *J Microbiol Immunol Infect*. 2020. https://doi.org/10.1016/j.jmii.2020.05.013.
2. Cucinotta D, Vanelli M. WHO declares COVID-19 a pandemic. *Acta Biomed*. 2020;91(1):157-160. https://doi.org/10.23750/abm.v91i1.9397.
3. Dong E, Du H, Gardner L. Coronavirus COVID-19 global cases by Johns Hopkins CSSE. *Lancet Infect Dis*. 2020. https://gisanddata.maps.arcgis.com/apps/opsdashboard/index.html/bda7594740fd40299423467b48e9ecf6.
4. Woelfel R, Corman VM, Guggemos W, et al. Clinical presentation and virological assessment of hospitalized cases of coronavirus disease 2019 in a travel-associated transmission cluster. medRXiv March 8, 2020
5. Bai Y, Yao L, Wei T, et al. Presumed asymptomatic carrier transmission of COVID-19. *JAMA*. 2020.
6. Forni G, Mantovani A. On behalf of the COVID-19 commission of Accademia Nazionale dei Lincei, Rome. et al. COVID-19 vaccines: where we stand and challenges ahead. *Cell Death Differ*. 2021;28:626-639. https://doi.org/10.1038/s41418-020-00720-9.
7. Zimmer C, Corum J, Wee S Coronavirus vaccine tracker; 2020. https://www.nytimes.com/interactive/2020/science/coronavirus-vaccine-tracker.html. Accessed March 03, 2021.
8. Terry M. Updated comparing COVID-19 vaccines: timelines, types and prices; 2021. https://www.biospace.com/article/comparing-covid-19-vaccines-pfizer-biontech-moderna-astrazeneca-oxford-j-and-j-russia-s-sputnik-v/. Accessed March 03, 2021.
9. WHO lists two additional COVID-19 vaccines for emergency use and Covax roll-out; 2021. https://www.who.int/news/item/15-02-2021-who-lists-two-additional-covid-19-vaccines-for-emergency-use-and-covax-roll-out. Accessed March 03, 2021.
10. BBC News, Coronavirus: the world in lockdown in maps and charts; April 7, 2020. https://www.bbc.com/news/world-52103747.
11. Tang B, Bragazzi NL, Li Q, Tang S, Xiao Y, Wu J. An updated estimation of the risk of transmission of the novel coronavirus (2019-nCov). *Infect Dis Model*. 2020;5:248-255.
12. Bjorgul K, Novicoff WM, Saleh KJ. Evaluating comorbidity in total hip and knee arthroplasty: available instruments. *J Orthop Traumatol*. 2010;11(4):203-209. https://doi.org/10.1007/s10195-010-0115-x.
13. Centres for Disease Control and Prevention (CDC) Coronavirus Disease 2019 (COVID-19); 2019. https://www.cdc.gov/coronavirus/2019-ncov/index.html.
14. Huang C, Wang Y, Li X, et al. Clinical features of patients infected with 2019 novel coronavirus in Wuhan, China. *Lancet*. 2020;395:497-506.
15. Wang D, Hu B, Hu C, et al. Clinical characteristics of 138 hospitalized patients with 2019 novel coronavirus-infected pneumonia in Wuhan, China. *JAMA*. 2020;323:1061-1069.
16. Yanga J, Zheng Y, Gou X, et al. Prevalence of comorbidity and its effects in patients infected with SARS-CoV-2: a systematic review and meta-analysis. *Int J Infect Dis*. 2020;94:91-95.
17. 70% of dead COVID-19 patients had diabetes, TB, hypertension- Ehanire; 2019. https://healthwise.punchng.com/70-of-dead-covid-19-patients-had-diabetes-tb-hypertension-ehanire/.

18. Dahiru T, Aliyu AA, Shehu AU. A review of population based studies on diabetes mellitus in Nigeria, Sub-Saharan African. *J Med.* 2016;3(2).

19. Okoye JO. Attitudinal, regional and sex related vulnerabilities to COVID-19: considerations for early flattening of curve in Nigeria. *Med J Islam Repub Iran.* 2020;34(61). https://doi.org/10.34171/mjiri.34.61.

20. Badawi A, Ryoo SG. Prevalence of diabetes in the 2009 influenza A (H1N1) and the Middle East respiratory syndrome coronavirus: a systematic review and meta-analysis. *J Public Health Res.* 2016;5(3):733-739.

21. Carey IM, Critchley JA, DeWilde S, Harris T, Hosking FJ, Cook DG. Risk of infection in type 1 and type 2 diabetes compared with the general population: a matched cohort study. *Diabetes Care.* 2018;41(3):513-521. https://doi.org/10.2337/dc17-2131.

22. WHO No evidence that recovered COVID-19 patients cannot be reinfected; 2019. https://news.un.org/en/story/2020/04/1062612.

23. Smith J. South Korea reports more recovered coronavirus patients testing positive again. https://www.reuters.com/article/us-health-coronavirus-southkorea/southkorea-reports-more-recovered-coronavirus-patients-testingpositive-again-idUSKCN21V0JQ. Accessed: August 20, 2020.

24. BBC News, Coronavirus: South Korea confirms second wave of infections; https://www.bbc.com/news/world-asia-53135626. Accessed: August 20, 2020

25. Euro News Debate, Beijing tightens controls as new coronavirus outbreak fans fear of second wave; 2020. https://www.euronews.com/2020/06/15/new-coronavirus-outbreak-in-china-fans-fears-of-second-wave.

26. Egonmwan AO, Okuonghae D. Mathematical analysis of a tuberculosis model with imperfect vaccine. *Int J Biomath.* 2019;12(7):1950073.

27. Odionyenma UB, Omame A, Ukanwoke NO, Nometa I. Optimal control of chlamydia model with vaccination. *Int J Dynam Control.* 2021. https://doi.org/10.1007/s40435-021-00789-1.

28. Nwankwo A, Okuonghae D. A mathematical model for the population dynamics of malaria with a temperature dependent control. *Differ Equ Dyn Syst.* 2019. https://doi.org/10.1007/s12591-019-00466-y.

29. Okuonghae D. Backward bifurcation of an epidemiological model with saturated incidence, isolation and treatment functions. *Qual Theory Dyn Syst.* 2019;18:413-440. https://doi.org/10.1007/s12346-018-0293-0.

30. Omame A, Okuonghae D, Umana RA, Inyama SC. Analysis of a co-infection model for HPV-TB. *Appl Math Model.* 2020;77:881-901.

31. Omame A, Okuonghae D, Inyama SC. A mathematical study of a model for HPV with two high-risk strains. In: Dutta H, ed. *Mathematical Modelling in Health, Social and Applied Sciences. Forum for Interdisciplinary Mathematics.* Vol 200. Singapore: Springer; 2020:107-149.

32. Omame A, Umana RA, Okuonghae D, Inyama SC. Mathematical analysis of a two-sex Human Papillomavirus (HPV) model. *Int J Biomath.* 2018;11(7):1850092

33. Omame A, Okuonghae D, Nwafor UE, Odionyenma BU. A co-infection model for HPV and syphilis with optimal control and cost-effectiveness analysis. *Int J Biomath.* 2021. https://doi.org/10.1142/S1793524521500509.

34. Sene N. Stability analysis of the generalized fractional differential equations with and without exogenous inputs. *J Nonlinear Sci Appl.* 2019;12:562-572.

35. Sene N. SIR epidemic model with Mittag-Leffler fractional derivative. *Chaos Soliton Fract.* 2020;137:109833.

36. Omame A, Inyama SC. Stochastic model and simulation of the prevalence of measles. *Int J Math Sci Eng.* 2014;8(1):311-323.

37. Umana RA, Omame A, Inyama SC. Deterministic and stochastic models of the dynamics of drug resistant tuberculosis. *FUTO J Ser.* 2016;2(2):173-194.

38. Egeonu KU, Omame A, Inyama SC. A co-infection model for two-strain Malaria and Cholera with optimal control. *Int J Dyn Cont.* 2021. https://doi.org/10.1007/s40435-020-00748-2.

39. Omame A, Nnanna CU, Inyama SC. Optimal control and cost-effectiveness analysis of an HPV-chlamydia trachomatis co-infection model. *Acta Biotheor.* 2021. https://doi.org/10.1007/s10441-020-09401-z.

40. Omame A, Okuonghae D. A co-infection model for oncogenic Human papillomavirus and tuberculosis with optimal control and cost-effectiveness analysis. *Optim Contr Appl Meth.* 2021. https://doi.org/10.1002/oca.2717.

41. Atangana A. Modelling the spread of COVID-19 with new fractal-fractional operators: can the lockdown save mankind before vaccination? *Chaos Soliton Fract.* 2020;136:109860.

42. Ferguson NM, Laydon D, Nedjati-Gilani G, et al. *Impact of Non-Pharmaceutical Interventions (NPIs) to Reduce COVID-19 Mortality and Healthcare Demand.* Vol 16. London, UK: Imperial College COVID-19 Response Team; 2020.

43. Mizumoto K, Chowell G. Transmission potential of the novel coronavirus (COVID-19) onboard the diamond princess cruises ship. *Infect Dis Model.* 2020;2020.

44. Okuonghae D, Omame A. Analysis of a mathematical model for COVID-19 population dynamics in Lagos, Nigeria. *Chaos Soliton Fract.* 2020;139:110032.

45. JKK A, Owusu MA, Jin Z, Oduro FT, Abidemi A, Gyasi EO. Global stability and cost-effectiveness analysis of COVID-19 considering the impact of the environment:using data from Ghana. *Chaos Soliton Fract.* 2020. https://doi.org/10.1016/j.chaos.2020.110103.

46. Nkwayep CH, Bowong S, Tewa JJ, Kurths J. Short-term forecasts of the COVID-19 pandemic: study case of Cameroon. *Chaos Soliton Fract.* 2020. https://doi.org/10.1016/j.chaos.2020.110106.

47. Lakshmikantham S, Leela S, Martynyuk AA. *Stability Analysis of Nonlinear Systems.* New York, NY: Marcel Dekker, Inc; 1989.

48. Hethcote HW. The mathematics of infectious diseases. *SIAM Rev.* 2000;42(4):599-653.

49. van den Driessche P, Watmough J. Reproduction numbers and sub-threshold endemic equilibria for compartmental models of disease transmission. *Math Biosci.* 2002;180:29-48.

50. Castillo-Chavez C, Song B. Dynamical models of tuberculosis and their applications. *Math Biosci Eng.* 2004;2:361-404.

51. La Salle J, Lefschetz S. *The Stability of Dynamical Systems.* Philadelphia, PA: SIAM; 1976.

52. World Population Review Lagos population 2020 (Demographics, Maps, Graphs); https://worldpopulationreview.com/world-cities/lagos-population/. Accessed April 25, 2020.

53. McCall J. Genetic algorithms for modelling and optimisation. *J Comput Appl Math*. 2005;184:205-222.

54. The Nigeria center for disease control; 2020. https://covid19.ncdc.gov.ng.

55. Life expectancy in Nigeria; 2020. https://www.worldometers.info/demographics/nigeria-demographics/#life-exp. Accessed June 24, 2020.

56. Chen T-M, Rui J, Wang Q-P, Zhao Z-Y, Cui J-A, Yin L. A mathematical model for simulating the phase-based transmissibility of a novel coronavirus. *Infect Dis Pov*. 2020;9(24). doi.org/10.1186/s40249-020-00640-3.

57. Pontryagin LS, Boltyanskii VG, Gamkrelidze RV, Mishchenko EF. *The Mathematical Theory of Optimal Processes*. New York, NY: Wiley; 1962.

58. Cantor SB, Ganiats TG. Incremental cost-effectiveness analysis: the optimal strategy depends on the strategy set. *Clin Epidemiol*. 1999;52(6):517-522.